ACS Catalysis

pubs.acs.org/acscatalysis Research Article

Hidden Role of Borane in Directed C−H Borylation: Rate Enhancement through Autocatalysis

Nghia Le, Natalie L. Chuang, Clay M. Oliver, Andrey V. Samoshin, Jack T. Hemphill, Kelsey C. Morris, Stephen N. Hyland, Hairong Guan,* Charles Edwin Webster,* and Timothy B. Clark*

Cite This: *ACS Catal.* 2023, 13, 12877−12893 Read Online

ACCESS | Metrics & More | Article Recommendations | Supporting Information

ABSTRACT: The metal-catalyzed C−H borylation reaction is a robust and valuable method for the installation of boronate esters into simple organic substrates. The regioselectivity observed in early examples was governed by steric control; those systems were extended to include a number of approaches that override the natural selectivity to obtain directed C−H borylation. In spite of the array of catalysts and directing groups that are now known to achieve directed reactions, no comprehensive experimental and computational study of the mechanism has been reported to date. In this study, experimental and computational results have been used to provide a detailed study of the catalytic mechanism of amine-directed C(sp^2)−H borylation. A notable result of the present study is the absence of inter- or intramolecular kinetic isotope effects at the functionalized C−H bond. The kinetic and computational data support a rate-determining reassociation of pinacolborane from the iridium catalyst to allow carbon−boron bond formation. An additional feature of note is the role of the boron source in the reaction. Computational analysis revealed the anticipated role of pinacolborane generated in the catalytic cycle. Based on this analysis, pinacolborane was examined as an additive, which overcame an induction period and provided an overall rate enhancement. Pinacolborane was found to serve as an autocatalyst in the transformation, a feature that can be utilized to improve the reactivity in directed C−H borylation reactions. The experimentally and computationally determined free energies of activation for the overall reaction are in agreement and provide valuable insights into substrate-directed C−H borylation reactions.

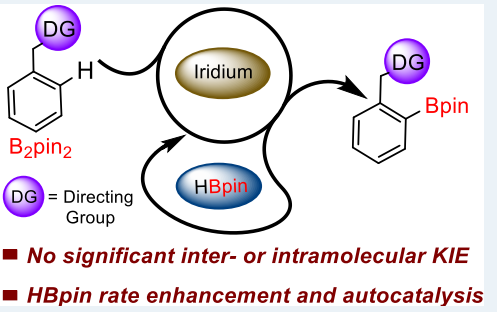

KEYWORDS: *C−H borylation, C−H functionalization, mechanism, kinetic isotope effect, autocatalytic, amine-directed*

INTRODUCTION

The metal-catalyzed C−H borylation reaction has received significant attention over the past two decades based on the efficiency and utility of converting unreactive C−H bonds into versatile and reactive C−B bonds.[1−4] Early catalytic reactions provided sterically controlled regioselectivity:[5−7] In the case of alkanes, primarily ruthenium and rhodium catalysts have been used to mediate the borylation of alkane C−H bonds, which is selective for primary C−H bonds.[8] For arenes, iridium has been employed most consistently, providing selectivity for C−H bonds without neighboring substituents. 1,3-Disubstituted and 1,2-symmetrically disubstituted arenes provide high regioselectivity, along with heteroarenes when there is a particularly reactive C−H bond.[6,9]

Since 2008, a significant focus of C−H borylation methods has been on the use of a directing group (DG) to provide complementary regioselectivity to the nondirected systems.[4,10−15] The predominant approach to achieve directed C−H borylation has relied on modifying the reported active catalyst for nondirected C−H borylation, an iridium(III) trisboryl complex (**I**, Figure 1) with a rigid bidentate ligand (bipyridine- or phenanthroline-based).[16−18] The rigid structure of the active catalyst limited early efforts to extend the method to directed C−H borylation based on the single open coordination site on the catalyst, which does not allow a traditional Lewis basic directing group to coordinate to the catalyst with an open coordination site remaining for C−H activation. Hartwig provided the first general example that overcame this limitation, using a silyl tether to direct ortho C−H borylation.[15,19] In this case, a silane, after a facile oxidative addition (Si−H bond)/reductive elimination (B−H bond) sequence, replaces one of the boryl ligands, maintaining the necessary reactivity in C−H borylation (**II**, Figure 1).

Silyl-directed C−H borylation initiated a wave of approaches to achieve directed C−H borylation,[4,10,12] including those that are directed to meta[20−28] or para C−H bonds.[29−34] While the diversity of approaches cannot be detailed in this report,[4] some

Received: July 19, 2023
Revised: August 28, 2023

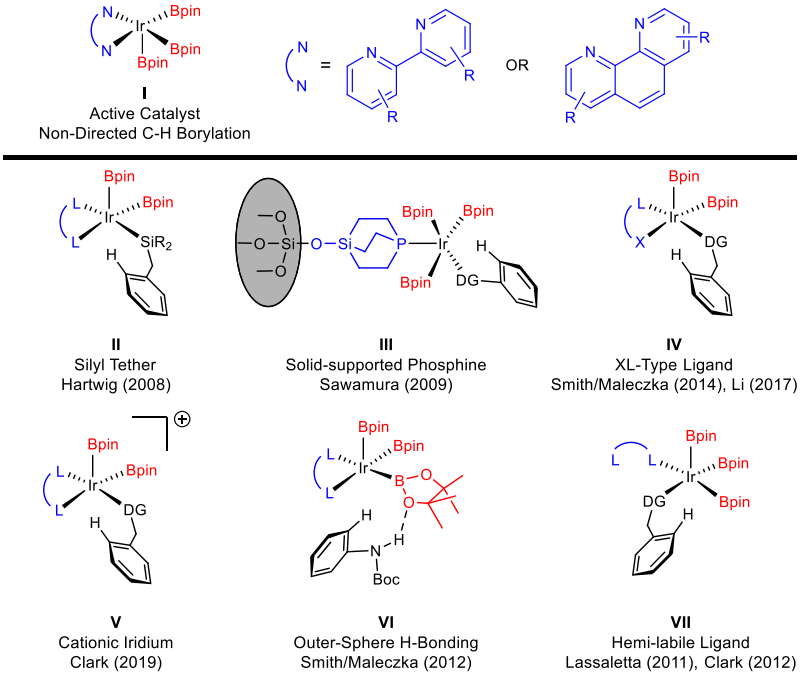

Figure 1. Major catalyst designs for substrate-directed C−H borylation.

Scheme 1. Experimentally and Computationally Supported Mechanisms for (a) Nondirected Iridium-Catalyzed C−H Borylation and (b) Amine-Directed C−H Borylation

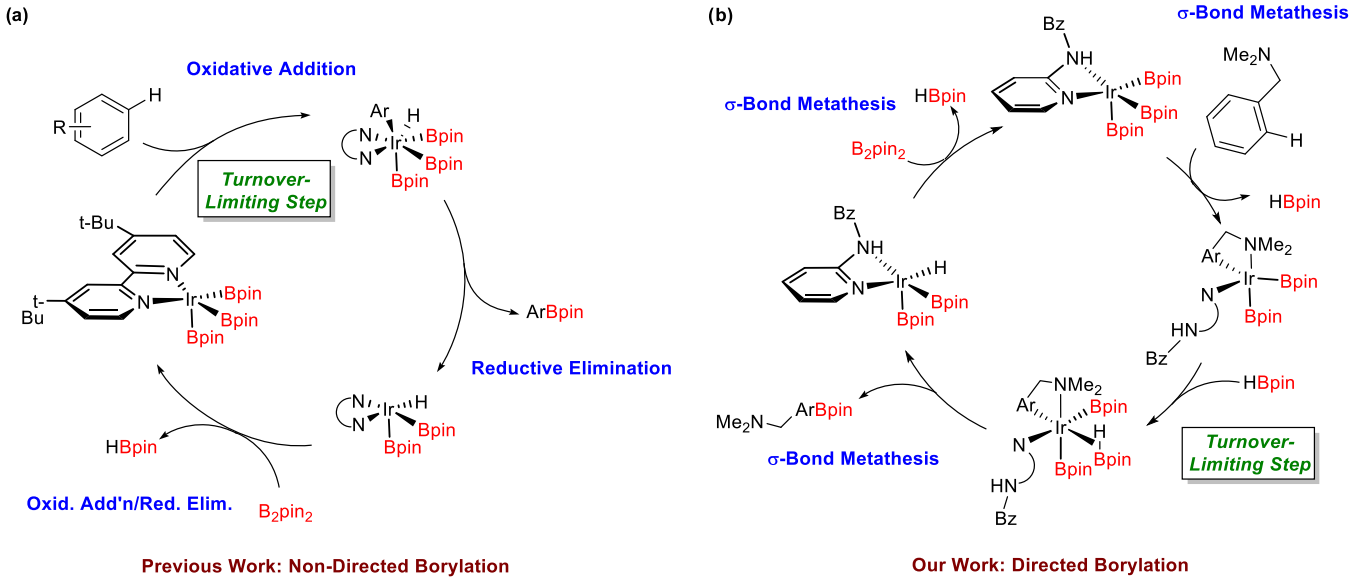

key approaches to ortho C−H borylation deserve mentioning. Sawamura developed solid-supported monodentate phosphine ligands which are believed to force the active catalyst to maintain two open coordination sites (**III**, Figure 1), providing a variety of directing groups that can mediate ortho C−H borylation.[35−37] Smith and Maleczka[38] and Li[39] developed rigid bidentate pro-ligands with a cleavable bond (e.g., Si−H or Si−B), which replaces one of the X-type boryl ligands on iridium (**IV**), opening an additional coordination site for Lewis basic directing groups. Chattopadhyay recently reported alternative pro-ligands that undergo cyclometalation with iridium to form C-/N-bound XL-type ligands while keeping two open coordination sites for directed C−H borylation.[40,41] Our group reported a parallel approach that uses a cationic iridium complex to open an additional coordination site for phosphine-directed C−H borylation (**V**).[42−47] Smith and Maleczka have also developed outer-sphere hydrogen bonding with the N−H of aniline carbamates (**VI**)[48,49] which has led to the use of a number of noncovalent interactions to achieve directed C−H borylation.[12,50,51] Lassaletta[52−54] and our group[55,56] have shown that hemilabile ligands can be used to temporarily open a coordination site for hydrazone- and amine-directed C−H borylation (**VII**).

In spite of the flurry of directed C−H borylation methods over the past decade, there has not been a comprehensive mechanistic study completed on any of the systems described above. Thus far, mechanistic work has been primarily theoretical, providing limited insights on a subset of

https://doi.org/10.1021/acscatal.3c03316
ACS Catal. 2023, 13, 12877−12893

Scheme 2. Context of C−H Borylation with No or Inverse Isotope Effect and Kinetic Dependence on Concentration of the Boron Sources

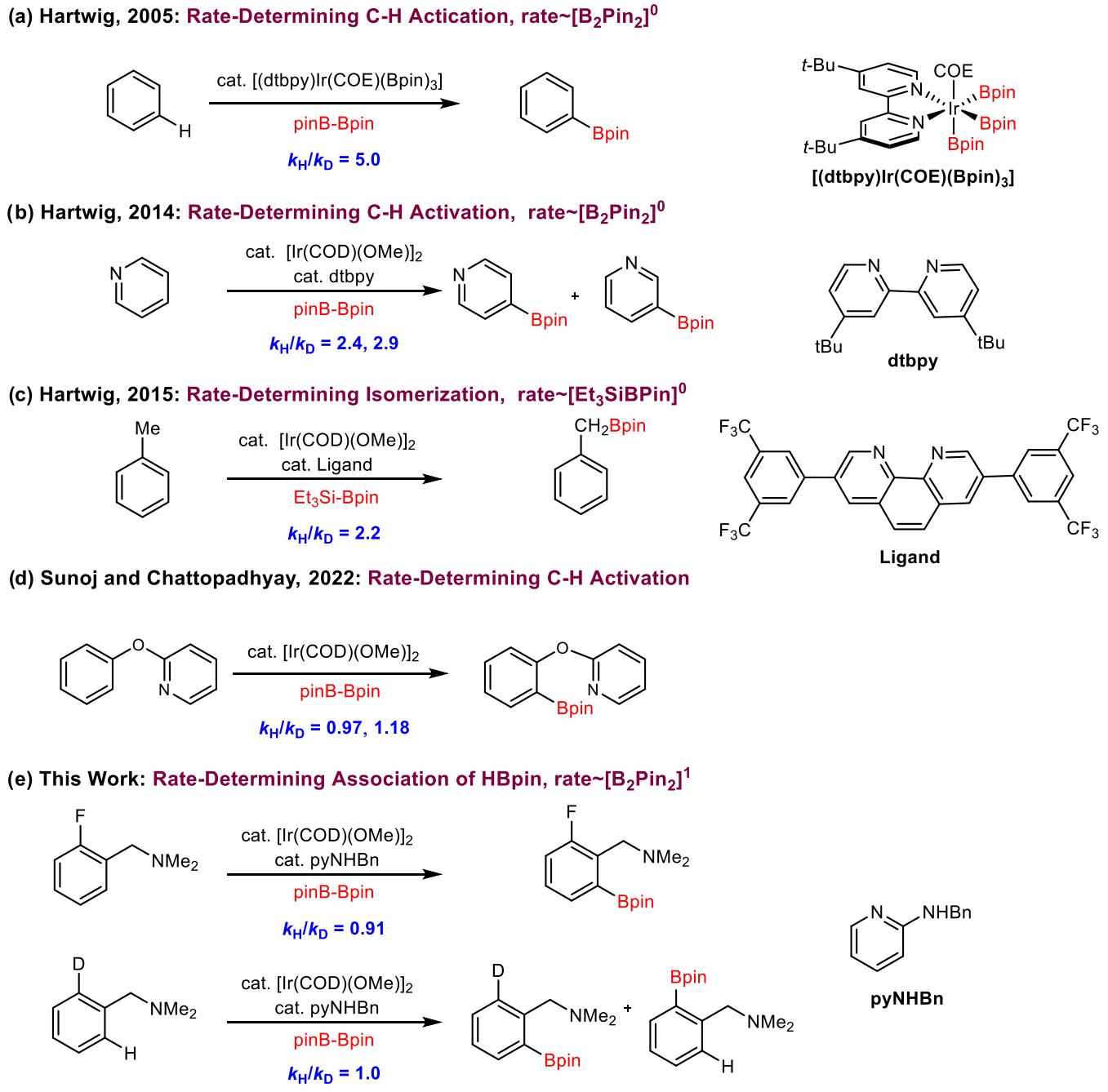

reactions.[40,50,57−63] We became interested in providing a greater understanding of this growing area of directed C−H borylation by conducting a full investigation into the mechanism of amine-directed C−H borylation using hemilabile ligands.[55,56] There have been two studies of directed C−H borylation that provide a context for our mechanistic investigation. The first one is a reaction that was studied computationally based on an ester-directed C−H borylation reported by Miyaura, which utilizes an electron-deficient monodentate phosphine, tris[3,5-bis(trifluoromethyl)phenyl]-phosphine with an $[Ir(\mu\text{-OMe})(COD)]_2$ precatalyst, to allow an ester to coordinate to iridium and maintain an open coordination site for C−H activation.[64] Jover and Maseras completed a detailed computational study that was consistent with the reactivity observed by Miyaura.[60] The second study was published by Sunoj and Chattopadhyay,[65] in which the reported transformation involved a ligand-free system for pyridine-directed C−H borylation of arenes. In this latter case, some experimental mechanistic studies were coupled with computational work to provide a more detailed picture of the mechanism.

Seminal studies on the mechanism of nondirected, iridium-catalyzed arene C−H borylation have been done computationally by Sakaki[66] and experimentally by Hartwig.[16] A simplified account of the catalytic cycle is provided in Scheme 1a, which highlights the rate-determining C−H activation of the arene by the iridium(III) trisboryl active catalyst.[16−18] In addition to the kinetic and computational evidence for this

https://doi.org/10.1021/acscatal.3c03316
ACS Catal. 2023, 13, 12877−12893

turnover-limiting step, the kinetic isotope effect (KIE) was determined by examining the catalytic C−H borylation of benzene and benzene-d_6 with a preformed iridium(III) trisboryl complex, running the two reactions in separate vessels to provide a large k_H/k_D of 5.0 (Scheme 2a). Stoichiometric reactions with the same catalyst gave a similar k_H/k_D (4.6). Two additional KIE studies were done by Hartwig on different types of substrates. The rate of C−H borylation of pyridine was compared to pyridine-d_5, providing a k_H/k_D of 2.9 for borylation in the 3-position and 2.4 in the 4-position (Scheme 2b).[67] The benzylic C−H borylation of toluene was also compared to toluene-d_8, resulting in a k_H/k_D of 2.2 (Scheme 2c).[68] In the recent work by Sunoj and Chattopadhyay on a ligand-free pyridine-directed C−H borylation, the intermolecular KIE depended on the extent of conversion and the precatalyst utilized, but nevertheless fell in the range of 0.97−1.18 (Scheme 2d).[65] It is important to note that, in all reported kinetic studies, the reaction rate is independent of the concentration of the boron source.[16,67,68]

Directed C−H borylation necessitates alternative mechanistic descriptions that account for the regiochemistry of the transformation. In the case of amine-directed C−H borylation, our initial proposed mechanism involved partial dissociation of a hemilabile diamine ligand.[55,56] Both experimental and computational experiments support this model and provide a detailed picture of the catalytic cycle that does not involve turnover-limiting C−H activation. Instead, isomerization of the C−H activated complex is the turnover-limiting step (see Scheme 1b for a summary of the proposed catalytic cycle). We herein report a detailed mechanistic study of this system that involves both experimental and computational insights into the amine-directed C−H borylation reaction. Turnover-limiting reassociation of pinacolborane (HBpin) has the highest free energy of activation in the regeneration of the active catalyst. HBpin, which is formed during the course of the reaction, also serves as an autocatalyst involving the slowest step. This study is highlighted by an unexpected inverse isotope effect on the activated C−H bond and no isotope effect in an intramolecular KIE study (Scheme 2e). Furthermore, different from previous kinetic studies, we provide an example in which a first-order dependence is observed for B_2Pin_2, which indicates that the directing group can alter the mechanism of C−H borylation.

EXPERIMENTAL AND COMPUTATIONAL DETAILS

All procedures involving air- or moisture-sensitive reagents were performed in oven- or flame-dried glassware and under purified nitrogen, either in an inert atmosphere glovebox or by standard Schlenk techniques. In all procedures, unless otherwise noted, the concentration was performed by rotary evaporation or by subjecting the material to high vacuum using a Schlenk line. Thin layer chromatography (TLC) analysis was performed on Whatman 60 Å silica layer fluorescence ultraviolet (UV) plates. Flash column chromatography was carried out on hand-packed columns of silica gel, 40−63 μm, 60 Å. NMR spectra were collected on a UNITY Inova spectrometer at 500 or 400 MHz for ^{1}H NMR, 125 or 100 MHz for ^{13}C NMR, 128 MHz for ^{11}B NMR. The ^{11}B NMR spectra were typically processed by adding 15 points of backward linear prediction to remove the glass peaks from the broadband probe and 5 Hz of apodization was applied. ^{1}H NMR spectra are referenced to $CDCl_3$ at 7.26 ppm, C_6D_6 at 7.16 ppm, tol-d_8 at 2.08 ppm, or to an internal tetramethylsilane (TMS) standard at 0.00 ppm. The ^{1}H NMR spectral data are reported as follows: chemical shift, parts per million; multiplicity (s = singlet, br s = broad singlet, d = doublet, t = triplet, q = quartet, qn = quintet, hex = hextet, sep = septet, oct = octet, m = multiplet), coupling constants (Hz), and integration. ^{13}C NMR spectra are referenced to $CDCl_3$ at 77.0 ppm or C_6D_6 at 128.0 ppm. Carbon atoms attached to boron are typically not observed and accounted for in the analysis. ^{11}B NMR spectra were referenced to an external $BF_3\cdot Et_2O$ sample in $CDCl_3$ or C_6D_6 (0.0 ppm). High-resolution mass spectrometry was obtained at the University of California, Irvine Mass Spectrometry Facility. All solvents were dried and degassed by standard procedures unless employed for extraction or purification. Dioxane and toluene were obtained from a solvent purification system, degassed by freeze−pump−thaw cycles (×3), and stored in the glovebox. Tetrahydrofuran was obtained from a solvent purification system, dried over sodium metal and benzophenone, distilled, followed by freeze−pump−thaw cycles (×3), and stored in the glovebox. Benzene-d_6 was distilled from CaH_2, degassed by freeze−pump−thaw cycles (×3), and stored in a glovebox. Chloroform-d was distilled from $MgSO_4$, degassed by freeze−pump−thaw cycles (×3), and stored in a glovebox. Bis(pinacolato)diboron, pinacolborane, di-μ-methoxobis(1,5-cyclooctadiene)diiridium(I), 2-benzylaminopyridine, phenyltrimethylsilane (PhTMS), *tert*-butyllithium solution (1.9 M in pentane), dimethylamine solution (40% in water), and all required benzyl bromides were purchased and employed without purification. Substrate **3** and aryl boronate ester **4** were synthesized as previously reported and matched spectral data.[55]

General Procedure for Kinetics Studies. All stock solutions used for kinetics were made with toluene-d_8 in the glovebox. Stock solutions of the di-μ-methoxobis(1,5-cyclooctadiene)diiridium(I) precatalyst, borylation substrate (with PhTMS as an internal standard), B_2pin_2, and 2-benzylaminopyridine were made using 1, 2, or 5 mL volumetric flasks. The solution of the precatalyst was made fresh before any kinetics experiments, as old solutions showed drastic and unpredictable changes in reaction rate. The stock solutions were made to the concentrations shown in Table S1 unless the total volume of the reaction mixture exceeded 0.600 mL. In those cases, the ligand solution was made more concentrated. The PhTMS internal standard was always included in the substrate solution to minimize addition errors.

Kinetics trials were done in triplicate or quadruplicate using the corresponding number of NMR tubes equipped with Teflon screwcaps (J-Young tubes). Microliter syringes were used to add stock solutions of each reagent to the J-Young tubes. Stock solutions were always added in the order: substrate **3** (with PhTMS internal standard), iridium precatalyst, 2-benzylaminopyridine, B_2pin_2, HBpin (if added), and toluene-d_8 to make up a total volume of 0.600 mL. Once mixed, the samples were sealed with Teflon screwcaps and removed from the glovebox. The samples were then placed into a 70 °C oil bath, which was maintained by a thermocouple stirring plate. A sample holder was made from a block of Teflon with 4 holes drilled to accommodate the NMR tubes. This sample holder allowed for operationally simple and reproducible placement of the samples in the oil bath. The samples were heated in the oil bath for a monitored amount of time. At the end of each heating interval, the samples were removed from the oil bath and promptly placed in an ice bath

https://doi.org/10.1021/acscatal.3c03316
ACS Catal. 2023, 13, 12877−12893

Scheme 3. Proposed Mechanism for the Iridium-Catalyzed C−H Borylation of Benzylic Amines

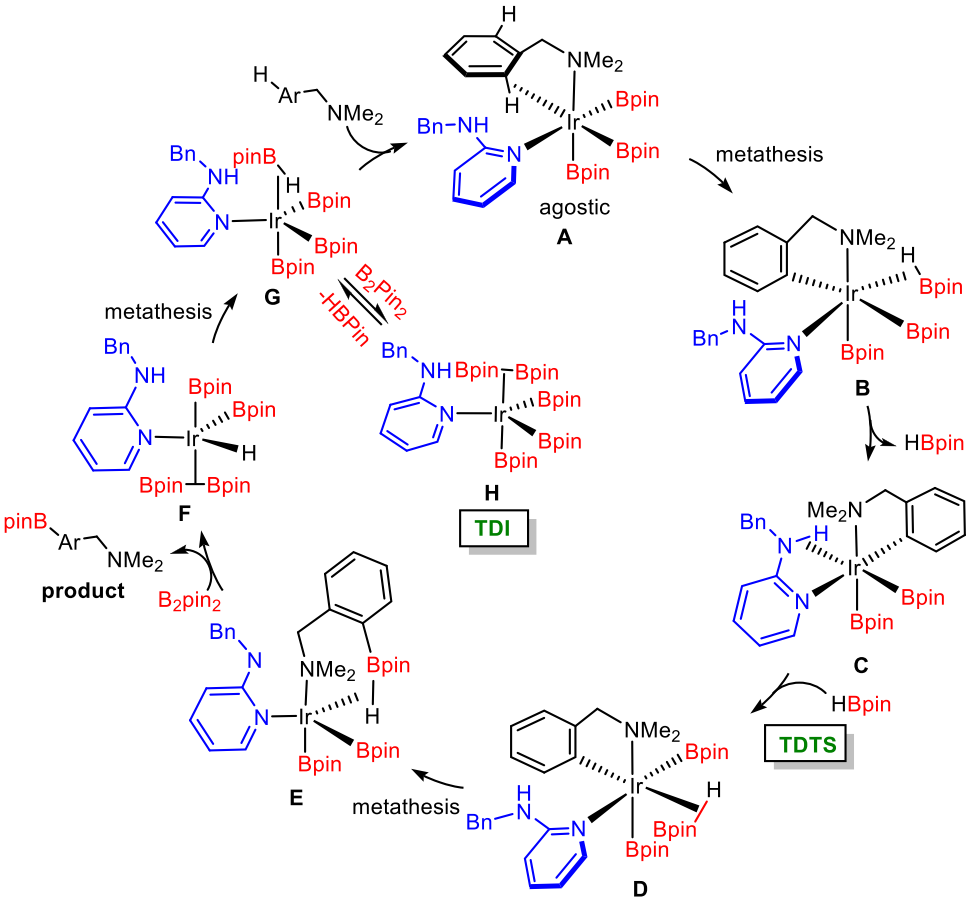

to halt the progression of the reaction while NMR spectra were acquired.

Computational Methodologies. All reported geometries [minima and transition states (TSs)] were fully optimized utilizing the Gaussian 09 D.01[69] implementation of the PBE0[70] density functional with the D3 version of the Grimme[71] dispersion correction with Becke-Johnson damping with basis set BS1 (where BS1 is the electron core potential and modified LANL2DZ basis set[72−74] for iridium and the 6-31G(*d*′) basis sets[75−77] for the remaining atoms). TSs were located by a combination of direct TS and quadratic synchronous transit QST3 techniques followed by confirmation of minimums, which along with atomic displacements along the imaginary modes ensure located TSs connect to corresponding minima. Exploring the effects of solvent, in select cases, single-point solvation computations were also performed on gas-phase geometries utilizing the solvation model based on density (SMD)[78] implicit solvation model via the self-consistent reaction field (SCRF) with parameters consistent with toluene modeled as the solvent.

Hopmann has previously shown that the pure PBE functional[79,80] combined with D2 dispersion correction[81] and the integral equation formalism variant of the polarizable continuum solvation model (IEFPCM, commonly referred to as PCM)[82−84] produces the most accurate results for iridium organometallic reaction chemistry.[85] Hopmann also found that when increasing the basis set size from 6-311G(*d*,*p*) to 6-311+G(2*d*,2*p*) for nonmetallic atoms and LanL2DZ(*f*) to LanL2TZ(*f*) for iridium does not improve the results, in fact, it even worsens them! Therefore, single-point energy computations with this recommended functional/basis set combination were performed to study the activation free energy of the catalytic process. Due to the size of the system, we use PBE0-D3/BS1 to optimize gas-phase geometries of TDI and TDTS:PCM−PBEPBE-D2/BS2//PBE0-D3/BS1 in Scheme 15. BS2 is the LANL2DZ valence basis set with one *f*-polarization function[86] for iridium and the LANL2DZ effective core potential and the 6-311G(*d*,*p*) basis sets for the remaining atoms. As a matter of convenience, in selected cases in the text, the Pople notation has been truncated; e.g., SMD//PBE0-D3/BS1 explicitly means SMD(Toluene)-PBE0-D3/BS1//PBE0-D3/BS1.

RESULTS AND DISCUSSION

A summary of the experimental and computational mechanistic study is shown in the catalytic cycle depicted in Scheme 3. The directed borylation by the iridium catalyst begins at agostic complex **A** where the substrate coordinates to the metal center. Utilizing the *p* orbital of the boron center in Bpin, the complex undergoes a σ-bond metathesis step to activate the C−H bond and produce complex **B**. An isomerization process via dissociation of HBpin (**B** to **C**) followed by reassociation of HBpin (**C** to **D**) affords the appropriate proximity between the B_{pin} and C_{aryl} ligands for C−B bond formation. The association of HBpin with **C** was found to be the TDTS (TOF determining transition state from the energetic span model).[87] Then, another σ-bond metathesis occurs to form the C−B_{pin} bond to convert isomer **D** to the aryl borate product **E**. Next, a ligand exchange process with bis-

https://doi.org/10.1021/acscatal.3c03316
ACS Catal. 2023, 13, 12877−12893

Scheme 4. Isolation of Competent Precatalyst 2

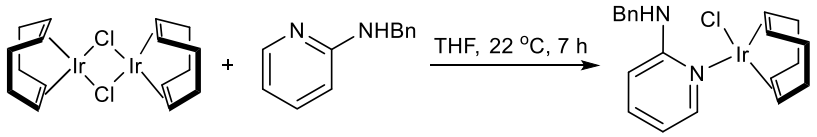

2, 100%

(pinacolato)diboron (B_2Pin_2) makes complex **F**. Finally, the tris-Bpin iridium species is regenerated by another σ-bond metathesis to yield complex **G**, a geometry with σ-bound HBpin, which was found to be TDI_c (TOF determining intermediate catalyst from the energetic span model). From complex **G**, either another equivalent of substrate can replace HBpin and start a new cycle or B_2Pin_2 can coordinate to the catalyst and produce stable complex **H**, which stays outside of the catalytic cycle and inhibits the reaction. Our experimental and computational evidence supporting the proposed mechanism will be discussed.

Attempted Isolation of Active Catalyst. Attempts to isolate an active catalyst for amine-directed C−H borylation were previously reported by our group as unsuccessful.[56] Addition of HBpin or B_2pin_2 and 2-benzylaminopyridine (the optimized ligand) to $[Ir(\mu\text{-OMe})(COD)]_2$ (complex **1**) in various orders of addition, as done by Ishiyama, Miyaura, and Hartwig,[16,88] and Smith and Maleczka[89] to synthesize iridium trisboryl complexes for nondirected systems,[16,88,89] provided complex mixtures impeding the synthesis of an active catalyst species (see the Supporting Information for spectra). Addition of 2-benzylaminopyridine to $[Ir(\mu\text{-Cl})(COD)]_2$ provided quantitative yield of square planar iridium(I) complex **2** (Scheme 4),[90] but attempts to form a boron-containing complex by the addition of HBpin or B_2pin_2 were unsuccessful. Complex **2** did, however, provide catalytic activity comparable to the separate addition of $[Ir(\mu\text{-Cl})(COD)]_2$ and 2-benzylaminopyridine in the presence of a boron source.[56] Going forward, $[Ir(\mu\text{-OMe})(COD)]_2$ was used as the precatalyst in all kinetic studies as it provides increased reaction efficiency over $[Ir(\mu\text{-Cl})(COD)]_2$ as the precatalyst. Our computational study also shows that $[Ir(\mu\text{-Cl})(COD)]_2$ leads to a more favorable isolated complex than the more common methoxy-substituted precatalyst $[Ir(\mu\text{-OMe})(COD)]_2$, see Scheme S9 in the SI.

Kinetic Studies of C−H Borylation of 2-Fluoro-*N*,*N*-dimethylbenzylamine—Reaction Order. Kinetic studies of the C−H borylation reaction were initiated on 2-fluoro-*N*,*N*-dimethylbenzylamine (**3**, Scheme 5); the *ortho*-fluorinated substrate was chosen to simplify the kinetics by limiting the number of reactive ortho C−H bonds, avoiding bis-ortho borylation. The reaction progress was monitored by ^{1}H NMR spectroscopy using the method of initial rates. The formation of aryl boronate ester **4** was monitored in a resealable NMR tube, primarily by comparing the appearance of the resonance at 1.26 ppm (ArBpin methyl hydrogens) with an internal phenyltrimethylsilane standard. The parent kinetic conditions were run with 0.2500 M **3**, 0.2500 M B_2pin_2, 0.0050 M $[Ir(\mu\text{-OMe})(COD)]_2$ (2 mol % $[Ir]_2$, 4 mol % Ir), and 0.0100 M 2-benzylaminopyridine (4 mol % pyNHBn) in toluene-d_8. A reaction temperature of 70 °C was used to provide reasonable reaction times at high and low concentrations of each reagent. All reactions were done in at least triplicate with at least 5 data points obtained through 15−20% conversion to **4**. A representative ^{1}H NMR spectra stackplot of a kinetic study is provided in the Supporting Information.

Scheme 5. Reaction Utilized to Study Kinetics

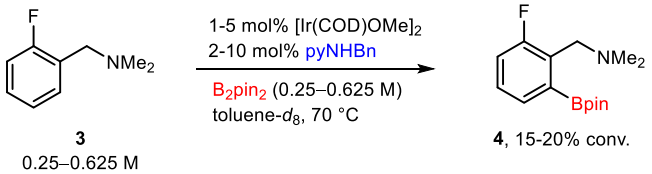

3
0.25–0.625 M

4, 15-20% conv.

The reaction order with respect to B_2pin_2 was interrogated by examining the kinetic profile at 0.2500, 0.3750, 0.5000, and 0.6250 M of $[B_2pin_2]$. As shown in Figure 2, the rates increased at a first-order dependence on the B_2pin_2 concentration, demonstrating that the rate law is first order in B_2pin_2 through this concentration regime.

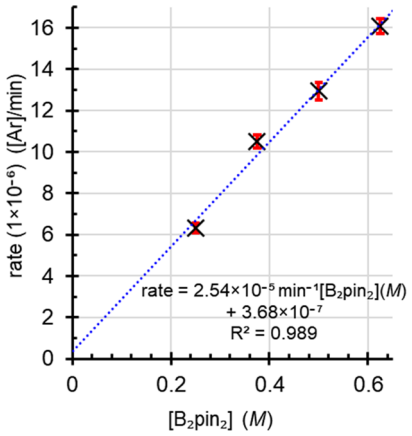

Figure 2. Kinetic plot of reaction rate (M/min) versus $[B_2pin_2]$ (M) from 0.2500 to 0.6250 M with 0.2500 M substrate **3**.

Identical concentration data points were obtained with varied concentrations of substrate **3** (0.2500 to 0.6250 M) and a 0.2500 M $[B_2pin_2]$ to examine the rate dependence on the substrate (Figure 3). In this case, the reaction is first order at low concentrations of substrate but results in saturation at higher concentrations of **3**.

The dependence of the rate on the catalyst loading was then examined. The 2:1 ratio of 2-benzylaminopyridine/**1** was maintained with each kinetic run, and the concentration of **1** was varied from 0.0025 M (2 mol % Ir) to 0.0125 M (10 mol % Ir). The reaction is first order in precatalyst concentration, shown in Figure 4 with the plot of the square root of the concentration of the iridium dimer, $\sqrt{[1]}$, versus rate of the reaction.

Effect of Pinacolborane on Kinetic Profile. Metal-catalyzed C−H borylation reactions predominantly utilize B_2pin_2 as the boron source. In some cases, however, HBpin is

https://doi.org/10.1021/acscatal.3c03316
ACS Catal. 2023, 13, 12877−12893

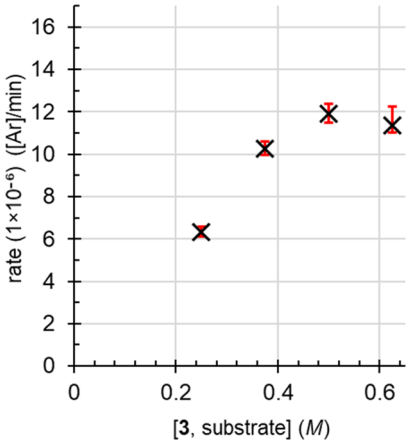

Figure 3. Kinetic plot of reaction rate (M/min) versus [**3**, substrate] (M) from 0.2500 to 0.6250 M with 0.2500 M B_2pin_2.

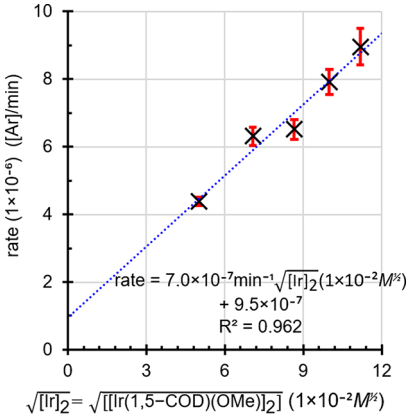

Figure 4. Kinetic plot of reaction rate (M/min) versus $\sqrt{[[Ir(\mu\text{-OMe})(COD)]_2]}$ ($M^{1/2}$) from 0.0025 to 0.0125 M of $[Ir]_2$ with 0.2500 M substrate **3** and B_2pin_2.

used as a catalytic additive, or as the sole boron source.[2,4,42,91] The reaction progress was therefore examined with varying combinations of B_2pin_2 and HBpin (Figure 5). Each reaction was heated to 90 °C followed by ^{1}H NMR spectroscopy using the method described for the kinetics experiments. The standard kinetics run (1 equiv of B_2pin_2) was followed for 250 min, resulting in a 70% NMR yield of **4**. Under these conditions, the ^{11}B NMR spectrum of the reaction mixture confirmed the presence of HBpin at 28.1 ppm. Over the course of the reaction, the formation of hydrogen gas was also observed in the ^{1}H NMR spectrum at 4.47 ppm (see the Supporting Information for ^{1}H and ^{11}B NMR spectra of the reaction over the course of the reaction). Furthermore, the presence of two metal hydride peaks was observed at −11.8 ppm (−11.79 and −11.85 ppm). We believe that these peaks represent σ-complexes of HBpin to iridium (such as **B**, **D**, and **G** in Scheme 3) and are consistent with an analogous σ-complex of HBpin to iridium reported by Heinekey with a chemical shift of −13.15 ppm.[92]

Addition of a catalytic amount of HBpin (0.1 equiv) to the reaction mixture provided a significant rate acceleration, reaching a similar amount of product formation in 80 min (66% NMR yield) and reaching 86% NMR yield after 250 min. The addition of a full equivalent of HBpin to the reaction mixture further accelerated the reaction, reaching 67% NMR yield in 60 min, and proceeding to ≥95% NMR yield in 140 min. The necessity of B_2pin_2 was then probed by adding HBpin as the sole boron source. With both 1 and 2 equiv of HBpin, the reaction was ineffective. Both reactions plateaued, resulting in 10% (1 equiv HBpin) and 22% NMR yield (2 equiv HBpin) after 200 min at 90 °C. Notably, when B_2Pin_2 is used as the sole boron source, there is an induction period that extends through 1200 s (see expansion in Figure 5). The induction period could result from the conversion of the dinuclear methoxide precatalyst to the active mononuclear iridium boryl species.[16,93]

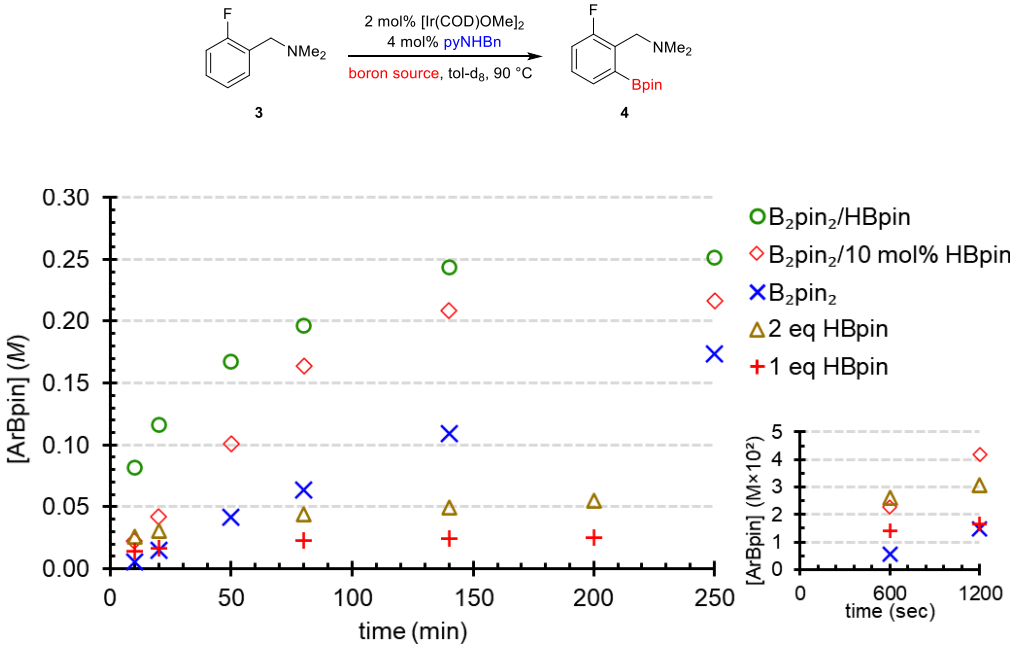

Figure 5. Kinetic profile of the formation of **4** with varying boron sources at 0.2500 M substrate **3** and 0.0050 M $[Ir]_2$.

https://doi.org/10.1021/acscatal.3c03316
ACS Catal. 2023, 13, 12877−12893

Scheme 6. Catalytic Reaction Used in the Computational Studies

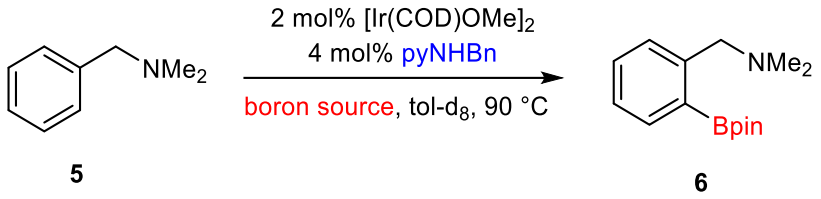

Scheme 7. Proposed Pathway for Amine-Directed C−H Borylation[a]

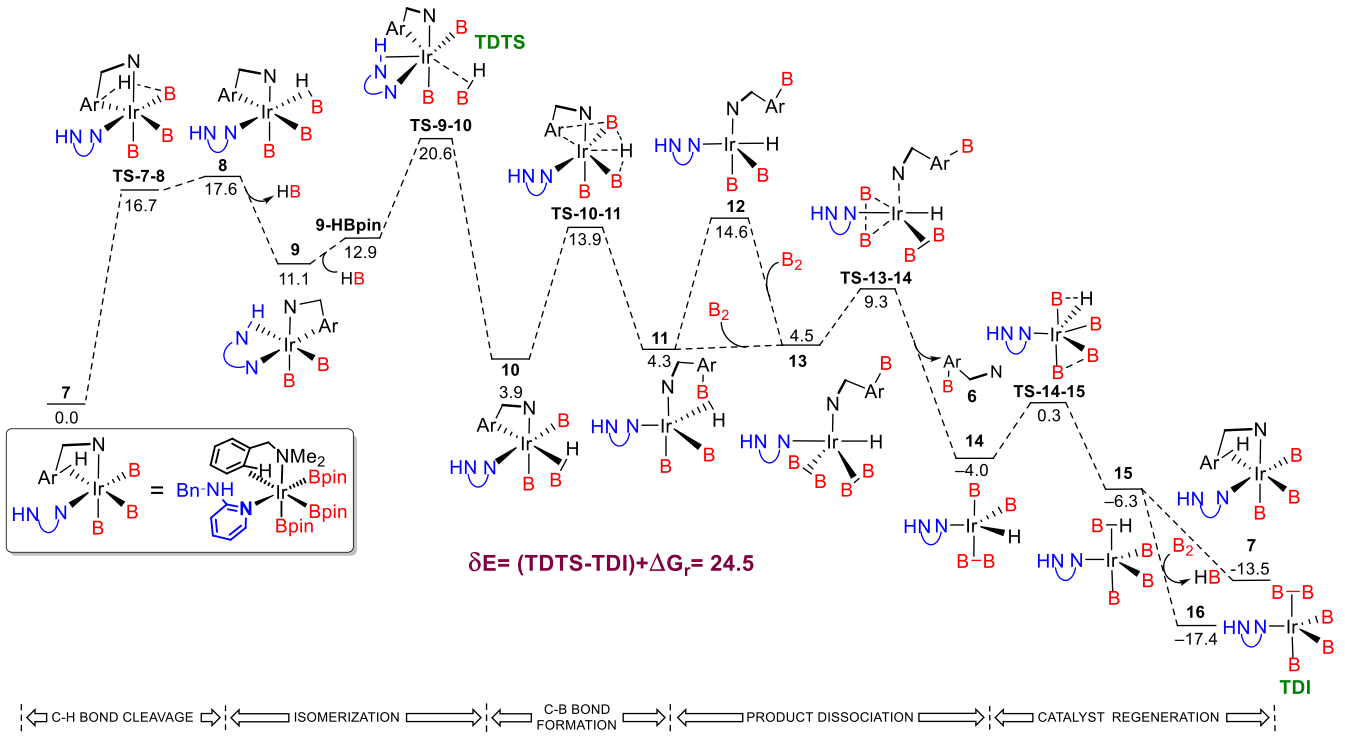

[a]Relative Gibbs free energies in kcal mol^{-1}.

COMPUTATIONAL STUDIES

Computed Energy Profile. The proposed mechanism for the amine-directed C−H borylation was derived from the results of density functional theory (DFT) computations. The system was modeled with benzylamine **5** as substrate, which produces the corresponding boronate ester **6** (Scheme 6).

Five key stages were identified in the reaction mechanism for the formation of the aryl boronate ester product (see Scheme 7): (1) C−H bond cleavage (complex **7** to complex **8**); (2) rate-determining isomerization of the iridium complex through dissociation and reassociation of HBpin (complex **8** to complex **10**); (3) C−B bond formation (complex **10** to complex **11**); (4) product dissociation (complex **11** to complex **14**); and (5) catalyst regeneration (complex **14** to complex **15**). The rate-determining association of HBpin with complex **9** (resulting from the dissociation of HBpin from complex **8**) is distinct from other experimental and computational work that typically involves rate-determining C−H activation. In this case, however, the σ-complex that results from C−H activation (i.e., complex **8**) does not have a low-energy C−B bond-forming step that is energetically accessible. The lowest-energy pathway requires dissociation of the HBpin (complex **8** to complex **9**), followed by reassociation in a location trans to the newly formed iridium−carbon bond (complex **9** to complex **10**). This isomerization allows for a low-energy transition state in forming the C−B bond.[94]

C−H Bond Cleavage. In previous computational studies of C−H borylation reactions, the key step is often the activation of the C−H bond. For example, Sakaki and co-workers reported a computational study on the iridium-catalyzed borylation of benzene with B_2pin_2 in which the C−H bond is broken in a rate-determining oxidative addition step.[66] Yao and co-workers also found that C−H oxidative addition step is the most energetically demanding process with a bulky ligand, leading to meta regioselectivity.[59] Both of these examples lack a directing group, which has the potential to alter the energy profile through the precoordination of the substrate to the iridium complex. The recent mechanistic work by Sunoj and Chattopadhyay, however, included computations for pyridine-directed C−H borylation. In their system, C−H activation was also shown to be the rate-determining step.[65]

Examination of complexes resulting from coordination of the benzylic amine to the iridium(III) trisboryl complex expected in this system resulted in low-energy complex **7** with an agostic interaction to the ortho C−H bond. The subsequent C−H activation step is no longer the highest point in the energy profile (Scheme 7), with a relative free energy of activation ($\Delta^{\ddagger}G^{\circ}$) of approximately 16.7 kcal/mol (for **TS-7−8**)

https://doi.org/10.1021/acscatal.3c03316
ACS Catal. 2023, 13, 12877−12893

Scheme 8. Computed Energies for C−H Activation from 7[a]

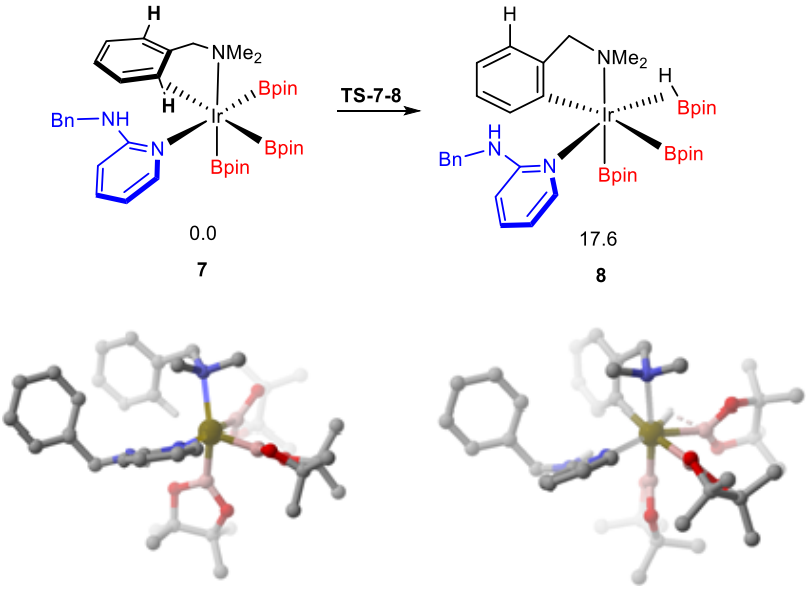

[a]Relative Gibbs free energies in kcal mol^{-1}.

compared to the highest free energy of activation of 20.6 kcal/mol (vide infra). A competing N−H bond activation was also considered but was found to have a significantly higher free energy of activation via **TS-7−17**, ($\Delta^{\ddagger}G^{\circ}$ = 25.8 kcal/mol; see S3.2 in the SI).

The key C−H bond activation step is known to undergo some form of two limiting mechanisms: (1) standard oxidative addition of the C−H bond, resulting in an iridium(V) complex;[66,68] (2) a σ-bond metathesis step that involves an interaction of the boron p-orbital, generating an iridium(III) complex with a B−H σ-complex.[68] In this case, the computed transition state proceeds through a σ-bond metathesis step, resulting in the direct formation of complex **8** (Scheme 8). The difference between metathesis and oxidative addition in this situation is a fundamental conceptual difference. If Ir(III) is oxidized to Ir(V) in the C−H bond cleavage step then the hydrogen bound to the iridium center would be a formal hydride ligand. However, in this case, the hydrogen is transferred through a σ-bond metathesis from the agostic C−H bond transferred directly to a σ-bound HBpin. Although most mechanistic studies for C−H borylation conclude an Ir(V) intermediate through standard oxidative addition, a closer look at the calculations is not decisively in favor of this mechanism for C−H activation. For example, Sakaki and co-worker calculations show that pentaboryl Ir(V) complex has one set of Bpin ligands that are closer in distance to each other than to the other Bpin group. Between those two boron atoms, d(B−B) is 2.1 Å and is significantly shorter than the other pair of cis Bpin ligands, d(B−B) from 2.5 to 2.8 Å.[66]

Isomerization. The typical mechanism for C−B bond formation in nondirected C−H borylation is reductive elimination from an iridium(V) complex.[16] The distinct feature in C−B bond formation in this system seems to result from the geometrical constraints imposed by the directing group, and therefore an isomerization process is required to accommodate the interaction between C_{aryl} and the boron of Bpin. The directing group makes the architecture more rigid and prohibits the formation of the C−B bond with the axial Bpin group due to a lack of proper orbital overlap without straining the five-membered ring metallacycle (Scheme 9).[95] Further attempts to force this C−B bond formation from

Scheme 9. Strain Caused by Directing Group for C−B Bond Formation

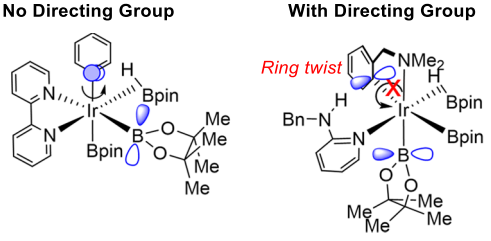

complexes **8** and **10** in a constrained potential energy surface also show these interactions are not accessible (see S3.3 in the SI).

Complex **10** was identified as the required isomer to achieve C−B bond formation with an accessible free energy of activation. To access isomer **10** (HBpin in the distal equatorial position) from complex **8** (initially formed upon C−H activation), several pathways were considered. Hartwig previously proposed internal isomerization by σ-bond metathesis transferring the hydride to an adjacent Bpin substituent.[16] In this case, however, the location of the hydride only allows formation of complex **18** with HBpin occupying the axial position, which has a higher free energy of activation to reductive elimination (vide infra; see Scheme 12). Hall and co-workers also reported the isomerization process by an HBpin dissociation pathway for a rigid pincer cobalt complex.[96] Applying this pathway to this system, HBpin completely dissociates from complex **8** and then recombines with a different orientation in order to form isomer **10**. The free energy for releasing HBpin is exergonic by 6.5 kcal/mol. However, this isomerization is quite a bit more complicated and involves a series of hydride relays in the proposed mechanism that lower the apparent free energy of activation and speeds up the reaction (see S3.4 in the SI).[97] The

https://doi.org/10.1021/acscatal.3c03316
ACS Catal. 2023, 13, 12877−12893

Scheme 10. Intermolecular Kinetic Isotope Effect Study

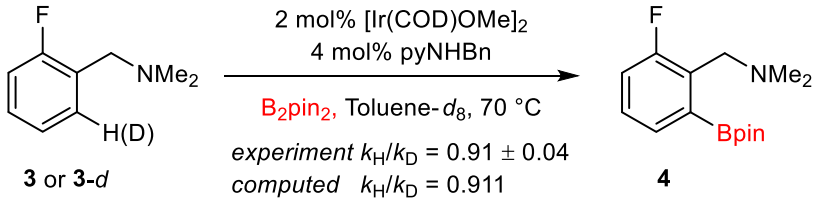

Scheme 11. Intramolecular Kinetic Isotope Effect Study

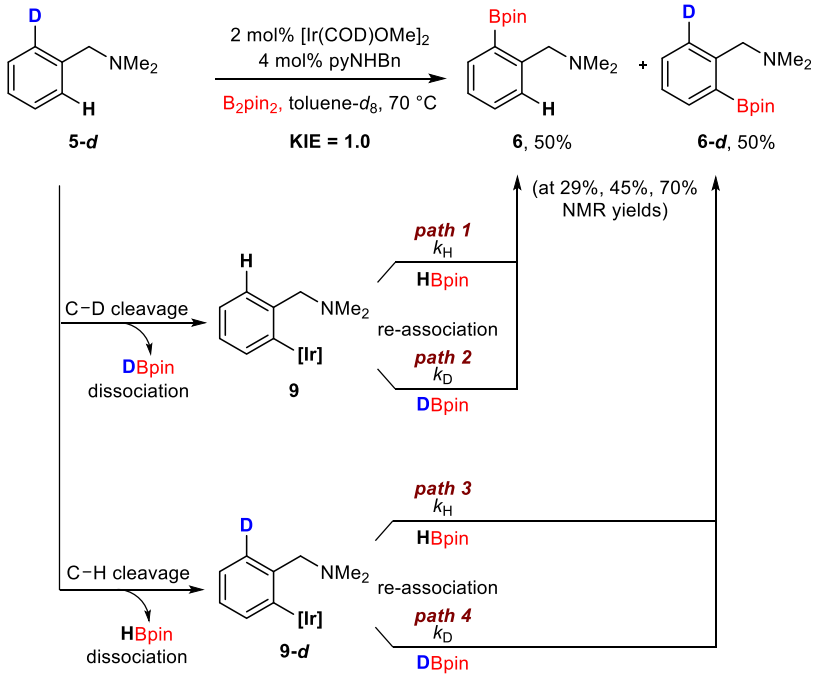

introduction of HBpin to complex **9** produces dipole−dipole complex **9-HBpin**. The transition state **TS-9−10** is the highest point in the energy profile, $\Delta^{\ddagger}G^{\circ}$ = 20.6 kcal/mol, and yields complex **10**, in which the aryl carbon and the boron are cis, with the orbitals aligned for C−B bond formation. Overall, the isomerization from complex **8** to complex **10** has a net Gibbs free energy, ΔG° = −13.7 kcal/mol, which illustrates a thermodynamically feasible process.

Kinetic Isotope Effect Studies. An intermolecular KIE was examined with 5-deutero-2-fluoro-*N*,*N*-dimethylbenzylamine (**3**-*d*) under the same reaction conditions used for the parent kinetic analysis (Scheme 10), providing a similar rate constant [(6.95 ± 0.21) × 10^{-6} M/s] to the protio sample [(6.33 ± 0.23) × 10^{-6} M/s]. The resulting k_H/k_D of 0.91 ± 0.04 is consistent with either a small inverse isotope effect or no isotope effect. A small inverse KIE was also observed by Sunoj and Chattopadhyay in their system.[65] The isotope effect in their study was attributed to the dominance of an equilibrium isotope effect (EIE) in the preequibrilium over KIE of TDTS (TOF determining transition state), which is the C−H bond activation. There are other examples in the literature showing that EIE is the main contribution to the observed inverse KIE.[98,99] However, omitting the primary KIE contribution in the slowest microscopic steps is questionable, especially those having isotopic labeled atoms involved significantly in motion in the TDTS such as C−H bond activation. In this study, we provide another interpretation of a small KIE without the contribution of EIE and based on examining the different mechanism in which HBpin reassociation is the TDTS. For the simulation of the KIE, TDI (TOF Determining Intermediate, complex **15**) and TDTS (**TS-9−10**) were used. Based on these stationary points, the intermolecular KIE simulation gives a fortuitously close k_H/k_D value of 0.911 when compared to 0.91 from the experiment. This value could be understood as an inverse secondary KIE. Within the **TS-9−10** transition state, the formation of an agostic B−H bond occurs, thus enabling a back-bonding interaction from Iridium to the σ^*(B−H). The interaction contribution from *p* and *d* orbitals results in analogous out-of-plane motion, which is similar to the well-known secondary isotope effect in sp^2 carbon centers.

An intramolecular KIE study was examined next, which typically will provide an isotope effect even if the C−H or C−D bond is not broken in the rate-determining step.[100] Deuterated substrate **5-*d*** was subjected to the reaction conditions (70 °C, 2 mol % $[Ir]_2$, 4 mol % ligand in toluene-d_8) and monitored throughout the reaction to 70% conversion of **5-*d*** to **6** and **6-*d*** (Scheme 11, moderate conversion was used to avoid bis-borylation products that are observed at high reaction conversion). The reaction was performed in triplicate and resulted in an intramolecular KIE of ∼1.0 at all time points examined (29, 45, and 70% NMR yield of **6** and **6-*d***). See the Supporting Information for details.

The fact that a difference between the intramolecular and intermolecular KIE is observed can be explained by the turnover-limiting step occurring after the C−H bond cleavage.

https://doi.org/10.1021/acscatal.3c03316
ACS Catal. 2023, 13, 12877−12893

Scheme 12. Carbon−Boron Bond Formation Transition States[a]

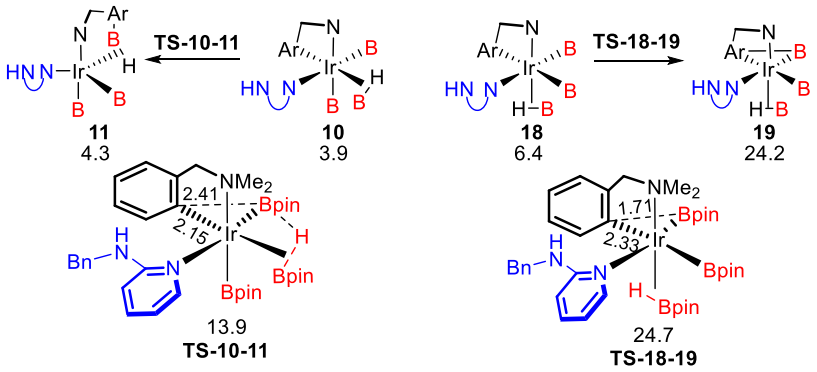

[a]Relative Gibbs free energies in kcal mol^{-1}.

Scheme 13. Possible Pathways for Dissociation of Borylated Arene from 12

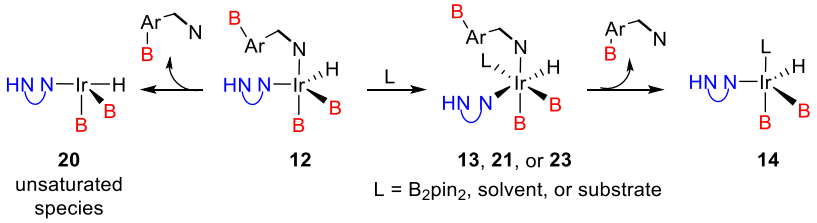

This observation is consistent with the current proposed mechanism in which HBpin dissociates and reassociates (complex **8** to complex **10**). Similar to the equilibrium between H- and D-substrates described in the work by Yi,[101] the recombination mechanism enables reactions to take place at hydrogen of **5-*d*** while still exhibiting a deuterium effect, and vice versa. As seen in Scheme 11, either HBpin or DBpin can be generated during the reaction with compound **5-*d***. In the reassociation step (**TS-9−10**, which is assigned to be the TDTS), either HBpin or DBpin can react with intermediate, complex **9**, or complex **9-*d***. Therefore, four different possibilities occur and form two different products, **6** and **6-*d*** in the intramolecular KIE experiment. It should be noted that the kinetic difference between substrate and deuterated substrate only comes from the HBpin or DBpin reassociation step. There is no differentiation made between complexes **9** and **9-*d*** because the motion in the imaginary mode of **TS-9−10** involves only the hydrogen or deuterium atom in HBpin or DBpin. As a result, the overall kinetic picture to produce product **6** will be the sum of *path 1* and *path 2* with $k = k_H + k_D$ and it is exactly the same value to create product **6-*d*** through the sum of *path 3* and *path 4*, $k = k_H + k_D$. Even though there is a difference in the zero-point energies between the two isotopic compounds, this cross reaction during the reassociation of HBpin or DBpin will cancel out the KIE in the intramolecular experiment. These results further affirm the dissociation and reassociation mechanistic proposal and demonstrate the unique mechanistic feature imposed by the directing group.

C−B Bond Formation. C−B bond formation requires one of the −Bpin groups to be adjacent to the Ir−C_{aryl} bond. The two isomers that meet this criterion with an equatorial-Bpin bond (complex **10** and complex **18**), were found to undergo reductive elimination with significantly different free energies of activation. Reductive elimination from complex **10** (**TS-10−11**) has a free energy of activation of 13.9 kcal/mol, whereas reductive elimination from complex **18** has a free energy of activation of 24.7 kcal/mol (Scheme 12). Complexes **10** and **18** are geometric isomers of each other with similar energies. The C−B bond formation transition states in Scheme 12 (**TS-10−11** and **TS-18−19**) are quite dissimilar: **TS-10−11** (with a B−C_{aryl} distance of 2.41 Å) is an earlier transition state in the direction of C−B bond formation than is **TS-18−19** (with a B−C_{aryl} distance of 1.71 Å, overlay structure in S3.2 in the SI). The products (complexes **11** and **19**) of the C−B bond formation transition states are also quite dissimilar. Complex **11** has an unusual stabilization of the bound product, with the metal-bound hydride strongly interacting with the boron of the product, essentially forming a borate with the B−H σ-bound to the iridium. From complex **11**, a subsequent transition state is required to break this boron−hydrogen interaction to form complex **12**, which has a nitrogen-bound product and a terminal hydride trans to the nitrogen of the pyridyl ligand (a hydride trans to the pyridyl nitrogen is lower in energy than other isomers here and throughout the computations). This spatial arrangement is consistent with the work of Fujita[102] and likely governed by the relative order of trans influence for the ligands involved: Bpin ≥ hydride ≥ pyridine ≥ tertiary amine.[103] Complex **19** has a nitrogen-bound product and a σ-bound H−Bpin.

Product Dissociation. Upon formation of complex **11** by reductive elimination, the desired C−B bond is installed, but the product remains bound to the iridium metal through both the nitrogen directing group and the newly installed Bpin group. Simple dissociation of the amine product would produce the unsaturated species (**20**, Scheme 13), which has a high free energy, ΔG° = 25.1 kcal/mol (see S3.5 in the SI) and, by necessity, an even higher free energy of activation. If this pathway were the only one for product formation, this TS would be the highest free energy point and would be the rate-determining step. Upon further examination, however, interactions with the solvent, substrate, or ligand were found

https://doi.org/10.1021/acscatal.3c03316
ACS Catal. 2023, 13, 12877−12893

to provide more stable complexes with lower free energies of activation so that this higher-energy species can be avoided. The dissociation pathway with an additional interaction from B_2Pin_2, solvent (toluene), or substrate (Me_2NBn) forms intermediates **13** (ΔG° = 4.5 kcal/mol, relative to **7**), **21** (ΔG° = 12.8 kcal/mol), or **23** (ΔG° = 16.2 kcal/mol), respectively. Coordination of B_2Pin_2 provides the lowest-energy path for product dissociation.

Catalyst Regeneration. The B_2pin_2-ligated complex **14** is poised for catalyst regeneration, which requires the net replacement of a hydride with a Bpin ligand. A low free energy activation σ-bond metathesis step was found to provide a low-energy pathway to complex **15** ($\Delta^{\ddagger}G^\circ$ = 0.3 kcal/mol), which has a σ-bonding interaction with H−Bpin and is the lowest-energy complex in the catalytic cycle (Scheme 14).

Scheme 14. Possible Pathways to Regenerate the Active Catalyst[a]

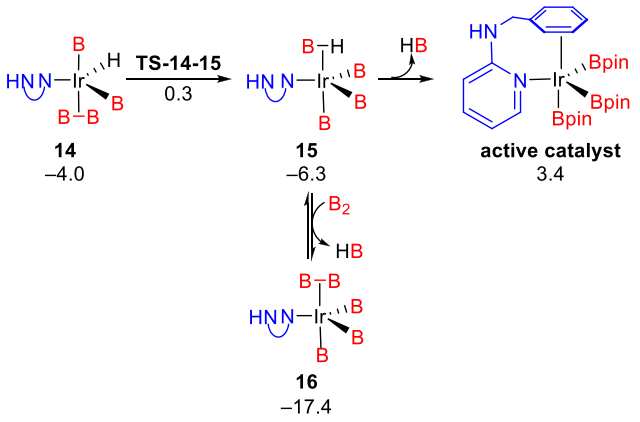

[a]Relative Gibbs free energies in kcal mol^{-1}.

There is an equilibrium where Me_2NBn replaces HBpin in complex **15** and starts the new cycle with regenerated complex **7** (**7′**), or dissociates HBpin and forms the active catalyst (ΔG° = 3.4 kcal/mol) before coordinating with Me_2NBn. The energy difference between complexes **7** and **7′** is the thermodynamic energy for the overall reaction after each cycle, ΔG_r = −13.5 kcal/mol (Scheme 7). The most stable complex **16**, produced by ligand exchange to replace σ-bound HBpin with σ-bound B_2Pin_2 (ΔG° = −17.4 kcal/mol), stays outside the catalytic cycle, can inhibit the catalyst regeneration process, and is assigned to turnover-limiting intermediate (TDI).

Rate Law and Effect of HBpin. According to our proposed mechanism, the steady-state approximation provides the following expression for the reaction rate: $= k[B_2pin_2][HBpin][substrate]\sqrt{[Ir]_2}$ as detailed in Section 2.5 in the SI. This expression shows first-order kinetics with respect to the concentrations of B_2Pin_2 and substrate (with saturation at higher concentrations) and half-order kinetics with respect to the concentration of the precatalyst. The saturation kinetics with respect to substrate **3** at higher concentrations of **3** can be explained by the necessary coordination of substrate **3** to the Iridium center leading to the formation of complex **7**, which is at low concentration (see Scheme 7). As the concentration of **3** continues to increase, however, there is no longer sufficient iridium complex remaining to bind to substrate **3** and increase the concentration of complex **7**.

In terms of the kinetic order of B_2Pin_2, although 1 equiv of B_2Pin_2 leads to the catalytic off-cycle species TDI, the catalytic process requires 2 equiv of B_2Pin_2 to regenerate the same TDI complex in the following turnover number (one for the reaction and one bound to the iridium center). In total, B_2pin_2 has a net order of 1 and is consistent with our kinetic measurements. This result is different from previously reported kinetic studies for nondirected borylation, in which the rate law was independent of the concentration of the boron source in all cases.[16,67,68] The observed half-order kinetics for the precatalyst suggests the existence of a reversible process between $[Ir(\mu\text{-OMe})(COD)]_2$ and trisboryliridium species, as previously reported by Hartwig and colleagues in their initial kinetic study.[16] Most importantly, the rate law includes the concentration of HBpin, which is a side product that explains the autocatalytic behavior. The HBpin concentration dependence of the rate law is consistent with the observation of an induction period (about 10 min) when no HBpin is added. When either HBpin is added or a high enough concentration of HBpin is generated, the reaction rate is accelerated.

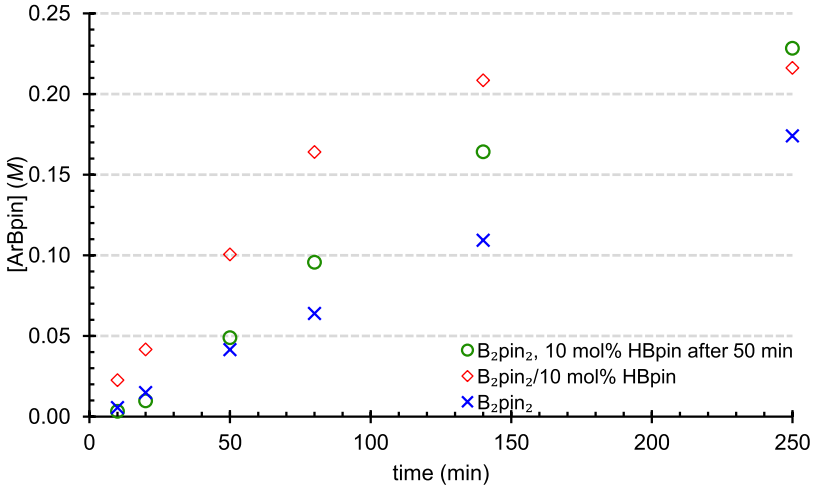

Figure 6. Kinetic profile of the formation of **4** with 10 mol % HBpin added at 50 min.

https://doi.org/10.1021/acscatal.3c03316
ACS Catal. 2023, 13, 12877−12893

Scheme 15. Comparison of the Experimental and Computational Kinetic Models and the Role of HBpin[a]

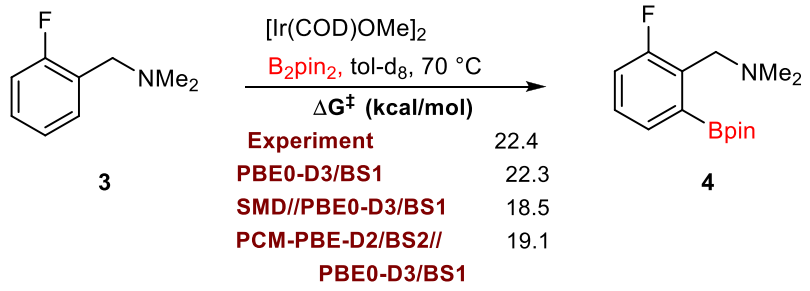

[a]Gibbs Free Energy of Activation is Given in kcal/mol.

To further support the role of HBpin as an autocatalyst and not merely involved in catalyst generation, a time course experiment was completed (Figure 6) that started with B_2pin_2 as the boron source (using the same conditions as those represented in Figure 5). After 50 min and a similar concentration of newly formed ArBpin **4**, 0.1 equiv of HBpin was added to the reaction. The rate of the reaction was immediately accelerated above the rate of the reaction with B_2pin_2 only. Because HBpin was added after the initiation period, the increased rate of the reaction is consistent with HBpin playing a role in the reaction mechanism outside of the initial generation of active catalyst.

Besides the autocatalytic effect of HBpin, other hypotheses were also considered: HBpin can be consumed as an independent boron source in the separated catalytic cycle or provides for a better energetic pathway in generating the active species. Because the addition of HBpin alone and B_2pin_2 alone are slower than the addition of both reagents and the rate acceleration with both reagents is much higher than the addition of HBpin alone (Figure 5), it is unlikely that the increased rate results from product formation through a second catalytic cycle. In terms of the possibility of precatalyst activation, from our computational analysis, HBpin does not provide a more favorable pathway for generating the active species compared to the B_2Pin_2 pathway (see S3.6 in the SI for more details).

Free Energy of Activation. The analogous computation was performed with monofluoro compound **3** to correlate the calculated free energy of activation to the experimental $\Delta^\circ G^\ddagger$ (Scheme 15). The kinetic experiments with substrate **3** further demonstrate the validity of this hypothesis and show that the experimentally determined free energy of activation (22.4 kcal/mol) is very close to the value computed at the PBE0-D3/BS1 level theory (22.3 kcal/mol).

To explore the computational effects of toluene as a solvent on the $\Delta^\circ G^\ddagger$, single-point SMD solvent model computations were performed by using gas-phase geometries. The results summarized in Table S2 show a good correlation ($R^2 = 0.966$) between the models with and without solvation (Figure S4). The same conclusions can be drawn about the mechanistic pathways. In terms of the DFT methodology, Hopmann's work shows that pure PBE functional combined with the D2 dispersion correction and the integral equation formalism variant of the polarizable continuum solvation model (IEFPCM) produces the most accurate results for iridium chemistry.[85] Thus, we report here a comparison with single-point computations using Hopmann's methodology (albeit on slightly different optimized geometries) using solvent parameters for toluene. In Scheme 15, it is interesting that the closest value was obtained by PBE0-D3/BS1 which is a gas phase and utilizes a double-ζ basis set. However, the computational results in general are in agreement with the experimental kinetic value, regardless of which methodology is used.

CONCLUSIONS

Experimental and computational studies were utilized to examine the mechanism of amine-directed C−H borylation. The turnover-limiting step of the catalytic cycle is the isomerization of the iridium(III) C−H-activated complex rather than the C−H activation step itself. This unusual outcome is supported by the lack of both inter- and intramolecular KIE, and by computational analysis that shows a low free energy of activation for C−H activation by σ-bond metathesis. The computationally determined turnover-limiting step involves the isomerization of the complex that results from C−H activation. That isomerization involves the dissociation and reassociation of HBpin to align the complex in a way that allows C−B bond formation. Prior to isomerization, an inaccessibly high free energy of activation is observed for C−B bond formation. The resulting computational energetic profile provides an overall free energy of activation that matches the experimental results very well.

There is a clear distinction between the mechanism of directed and nondirected C−H borylation reactions that are unveiled through this comprehensive mechanistic study. Coordination of the directing group results in changes in the rate-determining step of the catalytic cycle by constraining the geometry of the multiple transition states. Ultimately, this change in the energy profile of the reaction resulted in two key experimental observations that are strongly corroborated by the results from the computations. First, the inverse KIE for an intermolecular labeling study and no KIE for an intramolecular competition experiment. Second is the role of HBpin as an autocatalyst when B_2pin_2 is the sole boron source and to accelerate the reaction as an additive. The latter result has potential implications in a wide range of C−H borylation reactions as it could render ineffective transformations as efficient upon addition of borane. The details of the mechanism provided in this work are expected to provide critical new insights into directed C−H borylation reactions, a steadily expanding area of C−H functionalization reactions.

ASSOCIATED CONTENT

Supporting Information

The Supporting Information is available free of charge at https://pubs.acs.org/doi/10.1021/acscatal.3c03316.

https://doi.org/10.1021/acscatal.3c03316
ACS Catal. 2023, 13, 12877−12893

Procedures; characterization; spectral data; and computational details (PDF)

XYZ-coordinates (XYZ)

AUTHOR INFORMATION

Corresponding Authors

Hairong Guan − *Department of Chemistry, University of Cincinnati, Cincinnati, Ohio 45221-0172, United States;* orcid.org/0000-0002-4858-3159; Email: hairong.guan@uc.edu

Charles Edwin Webster − *Department of Chemistry, Mississippi State University, Mississippi State, Mississippi 39762-9573, United States;* orcid.org/0000-0002-6917-2957; Email: ewebster@chemistry.msstate.edu

Timothy B. Clark − *Department of Chemistry and Biochemistry, University of San Diego, San Diego, California 92110, United States;* orcid.org/0000-0003-1194-5205; Email: clarkt@sandiego.edu

Authors

Nghia Le − *Department of Chemistry, Mississippi State University, Mississippi State, Mississippi 39762-9573, United States*

Natalie L. Chuang − *Department of Chemistry and Biochemistry, University of San Diego, San Diego, California 92110, United States*

Clay M. Oliver − *Department of Chemistry and Biochemistry, University of San Diego, San Diego, California 92110, United States*

Andrey V. Samoshin − *Department of Chemistry and Biochemistry, University of San Diego, San Diego, California 92110, United States*

Jack T. Hemphill − *Department of Chemistry and Biochemistry, University of San Diego, San Diego, California 92110, United States*

Kelsey C. Morris − *Department of Chemistry and Biochemistry, University of San Diego, San Diego, California 92110, United States*

Stephen N. Hyland − *Department of Chemistry and Biochemistry, University of San Diego, San Diego, California 92110, United States*

Complete contact information is available at: https://pubs.acs.org/10.1021/acscatal.3c03316

Notes

The authors declare no competing financial interest.

ACKNOWLEDGMENTS

The authors thank the National Science Foundation (CHE-1800201, −2102552, −1151092, −1764307, −2102192, −2154645) and The Camille and Henry Dreyfus Foundation for funding this research. The computational work was completed with resources provided by the Mississippi State University High Performance Computing Collaboratory and the Mississippi Center for Supercomputing Research. C.M.O. thanks the Doheny Foundation and the Farrell Family, and K.C.M. and N.L.C. thank the Alice B. Hayes Science Scholarships for summer research fellowships through the University of San Diego.

REFERENCES

(1) Ishiyama, T.; Miyaura, N. Transition Metal-Catalyzed Borylation of Alkanes and Arenes via C-H Activation. *J. Organomet. Chem.* **2003**, *680*, 3−11, DOI: 10.1016/S0022-328X(03)00176-1.

(2) Mkhalid, I. A. I.; Barnard, J. H.; Marder, T. B.; Murphy, J. M.; Hartwig, J. F. C−H Activation for the Construction of C−B Bonds. *Chem. Rev.* **2010**, *110*, 890−931, DOI: 10.1021/cr900206p.

(3) Hartwig, J. F. Borylation and Silylation of C−H Bonds: A Platform for Diverse C−H Bond Functionalizations. *Acc. Chem. Res.* **2012**, *45*, 864−873, DOI: 10.1021/ar200206a.

(4) Xu, L.; Wang, G.; Zhang, S.; Wang, H.; Wang, L.; Liu, L.; Jiao, J.; Li, P. Recent Advances in Catalytic C-H Borylation Reactions. *Tetrahedron* **2017**, *73*, 7123−7157, DOI: 10.1016/j.tet.2017.11.005.

(5) Ishiyama, T.; Miyaura, N. Iridium-Catalyzed Borylation of Arenes and Heteroarenes via C-H Activation. *Pure Appl. Chem.* **2006**, *78*, 1369−1375, DOI: 10.1351/pac200678071369.

(6) Hartwig, J. F. Regioselectivity of the Borylation of Alkanes and Arenes. *Chem. Soc. Rev.* **2011**, *40*, 1992−2002, DOI: 10.1039/c0cs00156b.

(7) Hurst, T. E.; Macklin, T. K.; Becker, M.; Hartmann, E.; Kügel, W.; Parisienne-La Salle, J.-C.; Batsanov, A. S.; Marder, T. B.; Sniekus, V. Iridium-Catalyzed C-H Activation versus Directed *ortho* Metalation: Complementary Borylation of Aromatics and Heteroaromatics. *Chem. - Eur. J.* **2010**, *16*, 8155−8161, DOI: 10.1002/chem.201000401.

(8) Wei, C. S.; Jiménez-Hoyos, C. A.; Videa, M. F.; Hartwig, J. F.; Hall, M. B. Origins of the Selectivity for Borylation of Primary over Secondary C−H Bonds Catalyzed by Cp*-Rhodium Complexes. *J. Am. Chem. Soc.* **2010**, *132*, 3078−3091, DOI: 10.1021/ja909453g.

(9) Wright, J. S.; Scott, P. J. H.; Steel, P. G. Iridium-Catalysed C-H Borylation of Heteroarenes: Balancing Steric and Electronic Regiocontrol. *Angew. Chem., Int. Ed.* **2021**, *60*, 2796−2821, DOI: 10.1002/anie.202001520.

(10) Ros, A.; Fernández, R.; Lassaletta, J. M. Functional Group Directed C-H Borylation. *Chem. Soc. Rev.* **2014**, *43*, 3229−3243, DOI: 10.1039/C3CS60418G.

(11) Kuroda, Y.; Nakao, Y. Catalyst-Enabled Site-Selectivity in the Iridium-Catalyzed C-H Borylation of Arenes. *Chem. Lett.* **2019**, *48*, 1092−1100, DOI: 10.1246/cl.190372.

(12) Haldar, C.; Hoque, M. E.; Bisht, R.; Chattopadhyay, B. Concept of Ir-Catalyzed C-H Bond Activation/Borylation by Noncovalent Interaction. *Tetrahedron Lett.* **2018**, *59*, 1269−1277, DOI: 10.1016/j.tetlet.2018.01.098.

(13) Haldar, C.; Hoque, M. E.; Chaturvedi, J.; Hassan, M. M. M.; Chattopadhyay, B. Ir-Catalyzed Proximal and Distal C-H Borylation of Arenes. *Chem. Commun.* **2021**, *57*, 13059−13074, DOI: 10.1039/D1CC05104K.

(14) Bisht, R.; Haldar, C.; Hassan, M. M. M.; Hoque, M. E.; Chaturvedi, J.; Chattopadhyay, B. Metal-Catalysed C-H Bond Activation and Borylation. *Chem. Soc. Rev.* **2022**, *51*, 5042−5100, DOI: 10.1039/D1CS01012C.

(15) Boebel, T. A.; Hartwig, J. F. Silyl-Directed, Iridium-Catalyzed *ortho*-Borylation of Arenes. A One-Pot *ortho*-Borylation of Phenols, Arylamines, and Alkylarenes. *J. Am. Chem. Soc.* **2008**, *130*, 7534−7535, DOI: 10.1021/ja8015878.

(16) Boller, T. M.; Murphy, J. M.; Hapke, M.; Ishiyama, T.; Miyaura, N.; Hartwig, J. F. Mechanism of the Mild Functionalization of Arenes by Diboron Reagents Catalyzed by Iridium Complexes. Intermediacy and Chemistry of Bipyridine-Ligated Iridium Trisboryl Complexes. *J. Am. Chem. Soc.* **2005**, *127*, 14263−14278, DOI: 10.1021/ja053433g.

(17) Ghaffari, B.; Vanchura, B. A., II; Chotana, G. A.; Staples, R. J.; Holmes, D.; Maleczka, R. E., Jr.; Smith, M. R., III Reversible Borylene Formation from Ring Opening of Pinacolborane and Other Intermediates Generated from Five-Coordinate Tris-Boryl Complexes: Implications for Catalytic C-H Borylation. *Organometallics* **2015**, *34*, 4732−4740, DOI: 10.1021/acs.organomet.5b00525.

(18) Green, A. G.; Liu, P.; Merlic, C. A.; Houk, K. N. Distortion/Interaction Analysis Reveals the Origins of Selectivities in Iridium-Catalyzed C-H Borylation of Substituted Arenes and 5-Membered

Heterocycles. *J. Am. Chem. Soc.* **2014**, *136*, 4575−4583, DOI: 10.1021/ja411699u.
(19) Robbins, D. W.; Boebel, T. A.; Hartwig, J. F. Iridium-Catalyzed, Silyl-Directed Borylation of Nitrogen-Containing Heterocycles. *J. Am. Chem. Soc.* **2010**, *132*, 4068−4069, DOI: 10.1021/ja1006405.
(20) Davis, H. J.; Mihai, M. T.; Phipps, R. J. Ion Pair-Directed Regiocontrol in Transition-Metal Catalysis: A Meta-Selective C-H Borylation of Aromatic Quaternary Ammonium Salts. *J. Am. Chem. Soc.* **2016**, *138*, 12759−12762, DOI: 10.1021/jacs.6b08164.
(21) Davis, H. J.; Genov, G. R.; Phipps, R. J. *meta*-Selective C-H Borylation of Benzylamine-, Phenethylamine-, and Phenylpropylamine-Derived Amides Enabled by a Single Anionic Ligand. *Angew. Chem., Int. Ed.* **2017**, *56*, 13351−13355, DOI: 10.1002/anie.201708967.
(22) Bisht, R.; Chattopadhyay, B. Formal Ir-Catalyzed Ligand-Enabled Ortho and Meta Borylation of Aromatic Aldehydes via in Situ-Generated Imines. *J. Am. Chem. Soc.* **2016**, *138*, 84−87, DOI: 10.1021/jacs.5b11683.
(23) Kuninobu, Y.; Ida, H.; Nishi, M.; Kanai, M. A *meta*-Selective C-H Borylation Directed by a Secondary Interaction between Ligand and Substrate. *Nat. Chem.* **2015**, *7*, 712−717, DOI: 10.1038/nchem.2322.
(24) Yang, L.; Uemura, N.; Nakao, Y. meta-Selective C-H Borylation of Benzamides and Pyridines by an Iridium-Lewis Acid Bifunctional Catalyst. *J. Am. Chem. Soc.* **2019**, *141*, 7972−7979, DOI: 10.1021/jacs.9b03138.
(25) Genov, G. R.; Douthwaite, J. L.; Lahdenperä, A. S. K.; Gibson, D. C.; Phipps, R. J. Enantioselective Remote C-H Activation Directed by a Chiral Cation. *Science* **2020**, *367*, 1246−1251, DOI: 10.1126/science.aba1120.
(26) Bisht, R.; Hoque, M. E.; Chattopadhyay, B. Amide Effects in C-H Activation: Noncovalent Interactions with L-Shaped Ligand for *meta* Borylation of Aromatic Amides. *Angew. Chem., Int. Ed.* **2018**, *57*, 15762−15766, DOI: 10.1002/anie.201809929.
(27) Lee, B.; Mihai, M. T.; Stojalnikova, V.; Phipps, R. J. Ion-Pair-Directed Borylation of Aromatic Phosphonium Salts. *J. Org. Chem.* **2019**, *84*, 13124−13134, DOI: 10.1021/acs.joc.9b00878.
(28) Chaturvedi, J.; Haldar, C.; Bisht, R.; Pandey, G.; Chattopadhyay, B. Meta Selective C-H Borylation of Sterically Biased and Unbiased Substrates Directed by Electrostatic Interaction. *J. Am. Chem. Soc.* **2021**, *143*, 7604−7611, DOI: 10.1021/jacs.1c01770.
(29) Saito, Y.; Segawa, Y.; Itami, K. *para*-C-H Borylation of Benzene Derivatives by a Bulky Iridium Catalyst. *J. Am. Chem. Soc.* **2015**, *137*, 5193−5198, DOI: 10.1021/jacs.5b02052.
(30) Haines, B. E.; Saito, Y.; Segawa, Y.; Itami, K.; Musaev, D. G. Flexible Reaction Pocket on Bulky Diphosphine-Ir Complex Controls Regioselectivity in *para*-Selective C-H Borylation of Arenes. *ACS Catal.* **2016**, *6*, 7536−7546, DOI: 10.1021/acscatal.6b02317.
(31) Mihai, M. T.; Williams, B. D.; Phipps, R. J. Para-Selective C-H Borylation of Common Arene Building Blocks Enabled by Ion-Pairing with a Bulky Countercation. *J. Am. Chem. Soc.* **2019**, *141*, 15477−15482, DOI: 10.1021/jacs.9b07267.
(32) Yang, L.; Semba, K.; Nakao, Y. *para*-Selective C-H Borylation of (Hetero)Arenes by Cooperative Iridium/Aluminum Catalysis. *Angew. Chem., Int. Ed.* **2017**, *56*, 4853−4857, DOI: 10.1002/anie.201701238.
(33) Hoque, M. E.; Bisht, R.; Haldar, C.; Chattopadhyay, B. Noncovalent Interactions in Ir-Catalyzed C-H Activation: L-Shaped Ligand for Para-Selective Borylation of Aromatic Esters. *J. Am. Chem. Soc.* **2017**, *139*, 7745−7748, DOI: 10.1021/jacs.7b04490.
(34) Montero Bastidas, J. R.; Oleskey, T. J.; Miller, S. L.; Smith, M. R., III; Maleczka, R. E., Jr Para-Selective, Iridium-Catalyzed C-H Borylations of Sulfated Phenols, Benzyl Alcohols, and Anilines Directed by Ion-Pair Electrostatic Interactions. *J. Am. Chem. Soc.* **2019**, *141*, 15483−15487, DOI: 10.1021/jacs.9b08464.
(35) Kawamorita, S.; Miyazaki, T.; Ohmiya, H.; Iwai, T.; Sawamura, M. Rh-Catalyzed *Ortho*-Selective C−H Borylation of *N*-Functionalized Arenes with Silica-Supported Bridgehead Monophosphine Ligands. *J. Am. Chem. Soc.* **2011**, *133*, 19310−19313, DOI: 10.1021/ja208364a.
(36) Yamazaki, K.; Kawamorita, S.; Ohmiya, H.; Sawamura, M. Directed Ortho Borylation of Phenol Derivatives Catalyzed by a Silica-Supported Iridium Complex. *Org. Lett.* **2010**, *12*, 3978−3981, DOI: 10.1021/ol101493m.
(37) Kawamorita, S.; Ohmiya, H.; Hara, K.; Fukuoka, A.; Sawamura, M. Directed Ortho Borylation of Funtionalized Arenes Catalyzed by a Silica-Supported Compact Phosphine−Iridium System. *J. Am. Chem. Soc.* **2009**, *131*, 5058−5059, DOI: 10.1021/ja9008419.
(38) Ghaffari, B.; Preshlock, S. M.; Plattner, D. L.; Staples, R. J.; Maligres, P. E.; Krska, S. W.; Maleczka, R. E., Jr.; Smith, M. R., III Silyl Phosphorus and Nitrogen Donor Chelates for Homogeneous Ortho Borylation Catalysis. *J. Am. Chem. Soc.* **2014**, *136*, 14345−14348, DOI: 10.1021/ja506229s.
(39) Wang, G.; Liu, L.; Wang, H.; Ding, Y.-S.; Zhou, J.; Mao, S.; Li, P. N,B-Bidentate Boryl Ligand-Supported Iridium Catalyst for Efficient Functional-Group-Directed C-H Borylation. *J. Am. Chem. Soc.* **2017**, *139*, 91−94, DOI: 10.1021/jacs.6b11867.
(40) Hoque, M. E.; Hassan, M. M. M.; Chattopadhyay, B. Remarkably Efficient Iridium Catalysts for Directed C(sp^2)-H and C(sp^3)-H Borylation of Diverse Classes of Substrates. *J. Am. Chem. Soc.* **2021**, *143*, 5022−5037, DOI: 10.1021/jacs.0c13415.
(41) Hassan, M. M. M.; Hoque, M. E.; Dey, S.; Guria, S.; Roy, B.; Chattopadhyay, B. Iridium-Catalyzed Site-Selective Borylation of 8-Arylquinolines. *Synthesis* **2021**, *53*, 3333−3342, DOI: 10.1055/a-1506-3884.
(42) Wright, S. E.; Richardson-Solorzano, S.; Stewart, T. N.; Miller, C. D.; Morris, K. C.; Daley, C. J. A.; Clark, T. B. Accessing Ambiphilic Phosphine Boronates through C-H Borylation by an Unforseen Cationic Iridium Complex. *Angew. Chem., Int. Ed.* **2019**, *58*, 2834−2838, DOI: 10.1002/anie.201812857.
(43) Crawford, K. M.; Ramseyer, T. R.; Daley, C. J. A.; Clark, T. B. Phosphine-Directed C-H Borylation Reactions: Facile and Selective Access to Ambiphilic Phosphine Boronate Esters. *Angew. Chem., Int. Ed.* **2014**, *53*, 7589−7593, DOI: 10.1002/anie.201402868.
(44) Morris, K. C.; Wright, S. E.; Meyer, G. F.; Clark, T. B. Phosphine-Directed sp^3 C-H, C-O, and C-N Borylation. *J. Org. Chem.* **2020**, *85*, 14795−14801, DOI: 10.1021/acs.joc.0c01706.
(45) Auth, M. R.; McGarry, K. A.; Clark, T. B. Phosphorus-Directed C-H Borylation. *Adv. Synth. Catal.* **2021**, *363*, 2354−2365, DOI: 10.1002/adsc.202100173.
(46) Wen, J.; Wang, D.; Qian, J.; Wang, D.; Zhu, C.; Zhao, Y.; Shi, Z. Rhodium-Catalyzed P^{III}-Directed *ortho*-C−H Borylation of Arylphosphines. *Angew. Chem., Int. Ed.* **2019**, *58*, 2078−2082, DOI: 10.1002/anie.201813452.
(47) Fukuda, K.; Iwasawa, N.; Takaya, J. Ruthenium-Catalyzed ortho C−H Borylation of Arylphosphines. *Angew. Chem., Int. Ed.* **2019**, *58*, 2850−2853, DOI: 10.1002/anie.201813278.
(48) Roosen, P. C.; Kallepalli, V. A.; Chattopadhyay, B.; Singleton, D. A.; Maleczka, R. E., Jr.; Smith, M. R., III Outer-Sphere Direction in Iridium C−H Borylation. *J. Am. Chem. Soc.* **2012**, *134*, 11350−11353, DOI: 10.1021/ja303443m.
(49) Preshlock, S. M.; Plattner, D. L.; Maligres, P. E.; Krska, S. W.; Maleczka, R. E., Jr.; Smith, M. R., III A Traceless Directing Group for C-H Borylation. *Angew. Chem., Int. Ed.* **2013**, *52*, 12915−12919, DOI: 10.1002/anie.201306511.
(50) Chattopadhyay, B.; Dannatt, J. E.; Andujar-De Sanctis, I. L.; Gore, K. A.; Maleczka, R. E., Jr.; Singleton, D. A.; Smith, M. R., III Ir-Catalyzed ortho-Borylation of Phenols Directed by Substrate-Ligand Electrostatic Interactions: A Combined Experimental/in Silico Strategy for Optimizing Weak Interactions. *J. Am. Chem. Soc.* **2017**, *139*, 7864−7871, DOI: 10.1021/jacs.7b02232.
(51) Li, H. L.; Kuninobu, Y.; Kanai, M. Lewis Acid-Base Interaction-Controlled *ortho*-Selective C-H Borylation of Aryl Sulfides. *Angew. Chem., Int. Ed.* **2017**, *56*, 1495−1499, DOI: 10.1002/anie.201610041.
(52) Ros, A.; Estepa, B.; López-Rodríguez, R.; Álvarez, E.; Fernández, R.; Lassaletta, J. M. Use of Hemilabile N,N Ligands in Nitrogen-Directed Iridium-Catalyzed Borylations of Arenes. *Angew.*

Chem., Int. Ed. **2011**, *50*, 11724−11728, DOI: 10.1002/anie.201104544.
(53) López-Rodríguez, R.; Ros, A.; Fernández, R.; Lassaletta, J. M. Pinacolborane as the Boron Source in Nitrogen-Directed Borylations of Aromatic *N*,*N*-Dimethylhydrazones. *J. Org. Chem.* **2012**, *77*, 9915−9920, DOI: 10.1021/jo301965v.
(54) Ros, A.; López-Rodríguez, R.; Estepa, B.; Álvarez, E.; Fernández, R.; Lassaletta, J. M. Hydrazone as the Directing Group for Ir-Catalyzed Arene Diborylations and Sequential Functionalizations. *J. Am. Chem. Soc.* **2012**, *134*, 4573−4576, DOI: 10.1021/ja300308c.
(55) Roering, A. J.; Hale, L. V. A.; Squier, P. A.; Ringgold, M. A.; Wiederspan, E. R.; Clark, T. B. Iridium-Catalyzed, Substrate-Directed C-H Borylation Reactions of Benzylic Amines. *Org. Lett.* **2012**, *14*, 3558−3561, DOI: 10.1021/ol301635x.
(56) Hale, L. V. A.; McGarry, K. A.; Ringgold, M. A.; Clark, T. B. Role of Hemilabile Diamine Ligands in the Amine-Directed C−H Borylation of Arenes. *Organometallics* **2015**, *34*, 51−55, DOI: 10.1021/om5007837.
(57) Zhu, L.; Qi, X.; Li, Y.; Duan, M.; Zou, L.; Bai, R.; Lan, Y. Ir(III)/Ir(V) or Ir(I)/Ir(III) Catalytic Cycle? Steric-Effect-Controlled Mechanism for the *para*-C-H Borylation of Arenes. *Organometallics* **2017**, *36*, 2107−2115, DOI: 10.1021/acs.organomet.7b00151.
(58) Zhou, J.; Lee, C.-I.; Ozerov, O. V. Computational Study of the Mechanism of Dehydrogenative Borylation of Terminal Alkynes by SiNN Iridium Complexes. *ACS Catal.* **2018**, *8*, 536−545, DOI: 10.1021/acscatal.7b03835.
(59) Liu, Y.; Chen, J.; Zhan, K.; Shen, Y.; Gao, H.; Yao, L. Mechanistic Study of the Ligand Controlled Regioselectivity in Iridium Catalyzed C-H Borylation of Aromatic Imines. *RSC Adv.* **2018**, *8*, 35453−35460, DOI: 10.1039/C8RA07886F.
(60) Jover, J.; Maseras, F. Mechanistic Investigation of Iridium-Catalyzed C-H Borylation of Methyl Benzoate: Ligand Effects in Regioselectivity and Activity. *Organometallics* **2016**, *35*, 3221−3226, DOI: 10.1021/acs.organomet.6b00562.
(61) Unnikrishnan, A.; Sunoj, R. B. Iridium-Catalyzed Regioselective Borylation through C-H Activation and the Origin of Ligand-Dependent Regioselectivity Switching. *J. Org. Chem.* **2021**, *86*, 15618−15630, DOI: 10.1021/acs.joc.1c02126.
(62) Zou, X.; Li, Y.; Ke, Z.; Xu, S. Chiral Bidentate Boryl Ligand-Enabled Iridium-Catalyzed Enantioselective Dual C-H Borylation of Ferrocenes: Reaction Development and Mechanistic Insights. *ACS Catal.* **2022**, *12*, 1830−1840, DOI: 10.1021/acscatal.1c05299.
(63) Zhang, M.; Wu, H.; Yang, J.; Huang, G. A Computational Mechanistic Analysis of Iridium-Catalyzed C(sp^3)-H Borylation Reveals a One-Stone-Two-Birds Strategy to Enhance Catalytic Activity. *ACS Catal.* **2021**, *11*, 4833−4847, DOI: 10.1021/acscatal.1c00389.
(64) Ishiyama, T.; Isou, H.; Kikuchi, T.; Miyaura, N. *Ortho*-C−H Borylation of Benzoate Esters with Bis(pinacolato)diboron Catalyzed by Iridium−Phoshine Complexes. *Chem. Commun.* **2010**, *46*, 159−161, DOI: 10.1039/B910298A.
(65) Hassan, M. M. M.; Mondal, B.; Singh, S.; Haldar, C.; Chaturvedi, J.; Bisht, R.; Sunoj, R. B.; Chattopadhyay, B. Ir-Catalyzed Ligand-Free Directed C-H Borylation of Arenes and Pharmaceuticals: Detailed Mechanistic Understanding. *J. Org. Chem.* **2022**, *87*, 4360−4375, DOI: 10.1021/acs.joc.2c00046.
(66) Tamura, H.; Yamazaki, H.; Sato, H.; Sakaki, S. Iridium-Catalyzed Borylation of Benzene with Diboron. Theoretical Elucidation of Catalytic Cycle Including Unusual Iridium(V) Intermediate. *J. Am. Chem. Soc.* **2003**, *125*, 16114−16126, DOI: 10.1021/ja0302937.
(67) Larsen, M. A.; Hartwig, J. F. Iridium-Catalyzed C-H Borylation of Heteroarenes: Scope, Regioselectivity, Application to Late-Stage Functionalization, and Mechansim. *J. Am. Chem. Soc.* **2014**, *136*, 4287−4299, DOI: 10.1021/ja412563e.
(68) Larsen, M. A.; Wilson, C. V.; Hartwig, J. F. Iridium-Catalyzed Borylation of Primary Benzylic C-H Bonds without a Directing Group: Scope, Mechanism, and Origins of Selectivity. *J. Am. Chem. Soc.* **2015**, *137*, 8633−8643, DOI: 10.1021/jacs.5b04899.
(69) Frisch, M. J.; Trucks, G. W.; Schlegel, H. B.; Scuseria, G. E.; Robb, M. A.; Cheeseman, J. R.; Scalmani, G.; Barone, V.; Mennucci, B.; Petersoon, G. A.; et al. *Gaussian 09, Revision D.01*; Guassian. Inc.: Wallingford, CT, 2009.
(70) Adamo, C.; Barone, V. Toward reliable density functional methods without adjustable parameters: The PBE0 model. *J. Chem. Phys.* **1999**, *110*, 6158−6170, DOI: 10.1063/1.478522.
(71) Grimme, S.; Antony, J.; Ehrlich, S.; Krieg, H. A Consistent and Accurate *ab initio* Parameterization of Denisty Functional Dispersion Correction (DFT-D) for the 94 Elements H-Pu. *J. Chem. Phys.* **2010**, *132*, No. 154104, DOI: 10.1063/1.3382344.
(72) Hay, P. J.; Wadt, W. R. Ab initio effective core potentials for molecular calculations. Potentials for K to Au including the outermost core orbitals. *J. Chem. Phys.* **1985**, *82*, 299−310, DOI: 10.1063/1.448975.
(73) Hay, P. J.; Wadt, W. R. Ab initio effective core potentials for molecular calculations. Potentials for the transition metal atoms Sc to Hg. *J. Chem. Phys.* **1985**, *82*, 270−283, DOI: 10.1063/1.448799.
(74) Couty, M.; Hall, M. B. Basis sets for transition metals: Optimized outer *p* functions. *J. Comput. Chem.* **1996**, *17*, 1359−1370.
(75) Hariharan, P. C.; Pople, J. A. The Influence of Polarization Functions on Molecular Orbital Hydrogenation Energies. *Theor. Chim. Acta* **1973**, *28*, 213−222, DOI: 10.1007/BF00533485.
(76) Petersson, G. A.; Al-Laham, M. A. A Complete Basis Set Model Chemistry. II. Open-Shell Systems and the Total Energies fo the First-Row Atoms. *J. Chem. Phys.* **1991**, *94*, 6081−6090, DOI: 10.1063/1.460447.
(77) Hehre, W. J.; Ditchfield, R.; Pople, J. A. Self-Consistent Molecular Orbital Methods. XII. Further Extensions of Gaussian-Type Basis Sets for Use in Molecular Orbital Studies of Organic Molecules. *J. Chem. Phys.* **1972**, *56*, 2257−2261, DOI: 10.1063/1.1677527.
(78) Marenich, A. V.; Cramer, C. J.; Truhlar, D. G. Universal Solvation Model Based on Solute Electron Density and on a Continuum Model of the Solvent Defined by the Bulk Dielectric Constant and Atomic Surface Tensions. *J. Phys. Chem. B* **2009**, *113*, 6378−6396, DOI: 10.1021/jp810292n.
(79) Perdew, J. P.; Burke, K.; Ernzerhof, M. Generalized Gradient Approximation Made Simple. *Phys. Rev. Lett.* **1996**, *77*, 3865−3868, DOI: 10.1103/PhysRevLett.77.3865.
(80) Perdew, J. P.; Burke, K.; Ernzerhof, M. Generalized Gradient Approximation Made Simple [Phys. Rev. Lett. 77, 3865 (1996)]. *Phys. Rev. Lett.* **1997**, *78*, No. 1396, DOI: 10.1103/PhysRevLett.78.1396.
(81) Grimme, S. Semiempirical GGA-type density functional constructed with a long-range dispersion correction. *J. Comput. Chem.* **2006**, *27*, 1787−1799, DOI: 10.1002/jcc.20495.
(82) Cancès, E.; Mennucci, B.; Tomasi, J. A new integral equation formalism for the polarizable continuum model: Theoretical background and applications to isotropic and anisotropic dielectrics. *J. Chem. Phys.* **1997**, *107*, 3032−3041, DOI: 10.1063/1.474659.
(83) Tomasi, J.; Mennucci, B.; Cancès, E. The IEF version of the PCM solvation method: an overview of a new method addressed to study molecular solutes at the QM ab initio level. *J. Mol. Struct.* **1999**, *464*, 211−226, DOI: 10.1016/S0166-1280(98)00553-3.
(84) Tomasi, J.; Mennucci, B.; Cammi, R. Quantum Mechanical Continuum Solvation Models. *Chem. Rev.* **2005**, *105*, 2999−3094, DOI: 10.1021/cr9904009.
(85) Hopmann, K. H. How Accurate is DFT for Iridium-Mediated Chemistry? *Organometallics* **2016**, *35*, 3795−3807, DOI: 10.1021/acs.organomet.6b00377.
(86) Ehlers, A. W.; Böhme, M.; Dapprich, S.; Gobbi, A.; Höllwarth, A.; Jonas, V.; Köhler, K. F.; Stegmann, R.; Veldkamp, A.; Frenking, G. A set of f-polarization functions for pseudo-potential basis sets of the transition metals Sc-Cu, Y-Ag and La-Au. *Chem. Phys. Lett.* **1993**, *208*, 111−114, DOI: 10.1016/0009-2614(93)80086-5.

(87) Kozuch, S.; Shaik, S. How to Conceptualize Catalytic Cycles? The Energetic Span Model. *Acc. Chem. Res.* **2011**, *44*, 101−110, DOI: 10.1021/ar1000956.
(88) Ishiyama, T.; Takagi, J.; Hartwig, J. F.; Miyaura, N. A Stoichiometric Aromatic C−H Borylation Catalyzed by Iridium(I)/2,2′-Bibyridine Complexes at Room Temperature. *Angew. Chem., Int. Ed.* **2002**, *41*, 3056−3058.
(89) Chotana, G. A.; Vanchura, B. A., II; Tse, M. K.; Staples, R. J.; Maleczka, R. E., Jr.; Smith, M. R., III Getting the Sterics Just Right: A Five-Coordinate Iridium Trisboryl Complex that Reacts with C-H Bonds at Room Temperature. *Chem. Commun.* **2009**, 5731−5733, DOI: 10.1039/b914736e.
(90) Seechurn, C. C. C. J.; Sivakumar, V.; Satoskar, D.; Colacot, T. J. Iridium-Catalyzed C-H Borylation of Heterocycles Using an Overlooked 1,10-Phenanthroline Ligand: Reinventing the Catalytic Activity by Understanding the Solvent-Assisted Neutral to Cationic Switch. *Organometallics* **2014**, *33*, 3514−3522, DOI: 10.1021/om500420d.
(91) Preshlock, S. M.; Ghaffari, B.; Maligres, P. E.; Krska, S. W.; Maleczka, R. E., Jr.; Smith, M. R., III High-Throughput Optimization of Ir-Catalyzed C−H Borylation: A Tutorial for Practical Applications. *J. Am. Chem. Soc.* **2013**, *135*, 7572−7582, DOI: 10.1021/ja400295v.
(92) Hebden, T. J.; Denney, M. C.; Pons, V.; Piccoli, P. M. B.; Koetzle, T. F.; Schultz, A. J.; Kaminsky, W.; Goldberg, K. I.; Heinekey, D. M. σ-Borane Complexes of Iridium: Synthesis and Structural Characterization. *J. Am. Chem. Soc.* **2008**, *130*, 10812−10820, DOI: 10.1021/ja801898m.
(93) Ishiyama, T.; Takagi, J.; Ishida, K.; Miyaura, N.; Anastasi, N. R.; Hartwig, J. F. Mild Iridium-Catalyzed Borylation of Arenes. High Turnover Numbers, Room Temperature Reactions, and Isolation of a Potential Intermediate. *J. Am. Chem. Soc.* **2002**, *124*, 390−391, DOI: 10.1021/ja0173019.
(94) One result of the computations should be noted. σ-complex **8** has a higher Gibbs free energy than its connecting transition state, **TS-7−8**. The electronic energy of complex **8**, however, is lower than that of **TS-7−8**.
(95) Ghosh, R.; Emge, T. J.; Krogh-Jespersen, K.; Goldman, A. S. Combined Experimental and Computational Studies on Carbon-Carbon Reductive Elimination from Bis(hydrocarbyl) Complexes of (PCP)Ir. *J. Am. Chem. Soc.* **2008**, *130*, 11317−11327, DOI: 10.1021/ja800434r.
(96) Li, H.; Obligacion, J. V.; Chirik, P. J.; Hall, M. B. Cobalt Pincer Complexes in Catalytic C-H Borylation: The Pincer Ligand Flips Rather Than Dearomatizes. *ACS Catal.* **2018**, *8*, 10606−10618, DOI: 10.1021/acscatal.8b03146.
(97) Liu, Y.-h.; Jiang, Z.-J. Computational Understanding of Catalyst-Controlled Borylation of Fluoroarenes: Directed vs. Undirected Pathway. *RSC Adv.* **2020**, *10*, 19562−19569, DOI: 10.1039/D0RA03428B.
(98) Northcutt, T. O.; Wick, D. D.; Vetter, A. J.; Jones, W. D. Investigation of the Mechanism of Alkane Reductive Elimination and Skeletal Isomerization in Tp'Rh(CNneopentyl)(R)H Complexes: The Role of Alkane Complexes. *J. Am. Chem. Soc.* **2001**, *123*, 7257−7270, DOI: 10.1021/ja003944x.
(99) Churchill, D. G.; Janak, K. E.; Wittenberg, J. S.; Parkin, G. Normal and Inverse Primary Kinetic Deuterium Isotope Effects for C-H Bond Reductive Elimination and Oxidative Addition Reactions of Molybdenocene and Tungstenocene Complexes: Evidence for Benzene σ-Complex Intermediates. *J. Am. Chem. Soc.* **2003**, *125*, 1403−1420, DOI: 10.1021/ja027670k.
(100) Simmons, E. M.; Hartwig, J. F. On the Interpretation of Deuterium Kinetic Isotope Effects in C-H Bond Functionalization by Transition-Metal Complexes. *Angew. Chem., Int. Ed.* **2012**, *51*, 3066−3072, DOI: 10.1002/anie.201107334.
(101) Yi, C. S.; Zhang, J. Formation of Bicylcic Pyrroles from the Catalytic Coupling Reaction of 2,5-Disubstituted Pyrroles with Terminal Alkynes, Involving the Activation of Multiple C-H Bonds. *Chem. Commun.* **2008**, 2349−2351, DOI: 10.1039/b804263b.
(102) Garg, K.; Matsubara, Y.; Ertem, M. Z.; Lewandowska-Andralojc, A.; Sato, S.; Szalda, D. J.; Muckerman, J. T.; Fujita, E. Striking Differences in Properties of Geometric Isomers of $[Ir(tpy)(ppy)H]^+$: Experimental and Computational Studies of their Hydricities, Interaction with CO_2, and Photochemistry. *Angew. Chem.* **2015**, *127*, 14334−14338, DOI: 10.1002/ange.201506961.
(103) Liu, T.; Liu, Z.; Tang, L.; Li, J.; Yang, Z. Trans Influence of Boryl Ligands in CO_2 Hydrogenation on Ruthenium Complexes: Theoretical Prediction of Highly Active Catalysts for CO_2 Reduction. *Catalysts* **2021**, *11*, No. 1356, DOI: 10.3390/catal11111356.